

*PhD thesis*

# LHC Interaction region upgrade

*Riccardo de Maria*

CERN-THESIS-2008-079  
14/04/2008



2008

---

# Abstract

The thesis analyzes the interaction region of the Large Hadron Collider (LHC). It proposes, studies and compares several upgrade options. The interaction region is the part of the LHC that hosts the particle detectors which analyze the collisions. An upgrade of the interaction region can potentially increase the number of collision events and therefore it is possible to accumulate and study a larger set of experimental data.

The main object of study are the focus systems that consist of a set of magnets in charge of concentrating the particle beams in a small spot at the interaction points.

The thesis uses the methods of beam optics and beam dynamics to design new interaction regions. Two design schemes are compared with a detailed analysis of the performance of several implementations. The design of the layouts takes into account the technical limitations that will affect possible realizations.

Either analytical or numerical methods are used to evaluate the performance of the proposed layouts. The thesis presents new general methods that can be used for problems beyond the scope of the thesis. An analytical method has been developed for finding the intrinsic limitations of the focus systems. It allows to perform an exhaustive scan of the accessible parameter space and thus presents an efficient tool for guiding the design process. A numerical optimization routine and several enhancements have been implemented in MADX, a code for beam optics design. The routines simplify the solution of several optimization problems of beam optics.

Keywords: accelerators design, beam optics, beam dynamics.



# Abstract

Con questa tesi si è voluto approfondire lo studio della zona di interazione del Large Hadron Collider (LHC) allo scopo di proporre possibili soluzioni di sviluppo (upgrade) della macchina.

La zona di interazione è quella parte di LHC che contiene i rivelatori di particelle che analizzano le collisioni. Un upgrade della zona di interazione permetterebbe potenzialmente di aumentare il numero di eventi rilevabili nella singola collisione e quindi di accumulare e studiare una quantità più elevata di dati sperimentali.

L'oggetto principale dello studio sono i sistemi focalizzanti per le particelle che consistono in una serie di magneti capaci di concentrare i fasci convergenti in una piccola regione nel punto di interazione.

Questa tesi usa metodi della ottica e della dinamica dei fasci per progettare nuove zone di interazione. Sono stati confrontati due schemi tecnologici alternativi, ponendo particolare attenzione alle differenti limitazioni tecniche che possono diventare pregiudicanti al momento della realizzazione.

Per determinare le performance degli schemi proposti sono usati metodi analitici e numerici. La tesi presenta inoltre metodi generali applicabili in contesti diversi.

In particolare è stato sviluppato un metodo analitico per l'individuazione delle limitazioni intrinseche dei sistemi focalizzanti per particelle. Il metodo permette di effettuare una analisi completa dello spazio dei parametri accessibile e fornisce un efficiente strumento per la progettazione.

Un metodo numerico di ottimizzazione e diversi miglioramenti sono stati ideati e implementati al fine di potenziare il codice MADX per la progettazione degli acceleratori. Le modifiche introdotte rendono più facile la soluzione di diversi problemi di ottimizzazione dell'ottica dei fasci.

Parole chiavi: progetto di acceleratori, ottica dei fasci di particelle, dinamica dei fasci di particelle.

---

# Contents

<b>1</b>	<b>Introduction</b>	<b>11</b>
1.1	Synopsis . . . . .	11
1.2	Contributions associated with this thesis . . . . .	12
1.3	Acknowledgment . . . . .	12
<b>2</b>	<b>The LHC Upgrade</b>	<b>13</b>
2.1	Introduction . . . . .	13
2.2	The Large Hadron Collider . . . . .	13
2.2.1	Top energy . . . . .	15
2.2.2	Luminosity . . . . .	15
2.3	Peak luminosity . . . . .	16
2.3.1	Bunch intensity . . . . .	17
2.3.2	Number of bunches . . . . .	18
2.3.3	Transverse beam size at the IP . . . . .	19
2.3.4	Geometric reduction factor . . . . .	19
2.4	Conclusion . . . . .	22
<b>3</b>	<b>LHC interaction region layout</b>	<b>25</b>
3.1	Introduction . . . . .	25
3.2	Beam dynamics . . . . .	25
3.2.1	Transverse dynamics . . . . .	27
3.2.2	Linear dynamics . . . . .	28
3.2.3	Non linear perturbations . . . . .	31
3.2.4	Dispersion and chromatic effects . . . . .	32
3.3	Interaction region layout . . . . .	35
3.3.1	Detector area . . . . .	35
3.3.2	TAS . . . . .	36
3.3.3	IR Triplets . . . . .	36
3.3.4	Separation/recombination section . . . . .	40
3.3.5	Matching section . . . . .	42
3.3.6	Dispersion suppressor . . . . .	43

## Contents

---

3.4	Limitations of the nominal interaction region layout . . . . .	44
3.4.1	Aperture . . . . .	44
3.4.2	Field quality and long term stability . . . . .	45
3.4.3	Beam beam interactions and geometric reduction factor	46
3.4.4	Heat deposition . . . . .	48
3.4.5	Radiation damage . . . . .	48
3.4.6	Chromatic aberrations . . . . .	48
3.4.7	Matchability . . . . .	48
3.5	Conclusion . . . . .	49
<b>4</b>	<b>Dipole first layout</b>	<b>51</b>
4.1	Introduction . . . . .	51
4.2	Motivations . . . . .	51
4.3	Dipole first layout . . . . .	52
4.4	Collision optics . . . . .	53
4.5	Crossing scheme . . . . .	55
4.6	Mechanical aperture . . . . .	57
4.7	Chromaticity . . . . .	59
4.8	Dynamic aperture . . . . .	60
4.8.1	DA from measured errors . . . . .	62
4.8.2	Multipole by multipole analysis . . . . .	62
4.9	Squeeze . . . . .	67
4.10	Conclusion . . . . .	67
<b>5</b>	<b>Quadrupole first layouts</b>	<b>69</b>
5.1	Introduction . . . . .	69
5.2	Motivation . . . . .	69
5.3	Optimization of triplet layout . . . . .	69
5.3.1	Final focus design . . . . .	71
5.3.2	Parameters . . . . .	73
5.3.3	Approximation of the equations . . . . .	73
5.3.4	Normalization . . . . .	75
5.3.5	Scalings . . . . .	75
5.3.6	Parameter space . . . . .	78
5.4	Four flavors of quadrupole first layouts . . . . .	80
5.5	Crossing scheme . . . . .	85
5.6	Mechanical aperture . . . . .	86
5.7	Chromaticity . . . . .	88
5.8	Dynamic aperture . . . . .	88
5.9	Transition to injection . . . . .	91
5.10	Conclusion . . . . .	91

<b>6</b>	<b>Conclusions</b>	<b>93</b>
<b>A</b>	<b>Optimization tools for accelerator optics</b>	<b>95</b>
A.1	Introduction . . . . .	95
A.2	Optimization and least-sqaure fitting . . . . .	96
A.3	Singular value decomposition . . . . .	97
A.4	JACOBIAN algorithm . . . . .	98
A.5	Conclusion . . . . .	101

## Contents

---

# Chapter 1

## Introduction

### 1.1 Synopsis

The topic of the thesis concerns the upgrade of the Large Hadron Collider interaction region.

Chapter 2 presents an introduction of the LHC performance, limitations and upgrade strategies. The chapter concludes by identifying the upgrade of the interaction regions as a viable option for increasing the luminosity in the LHC by reducing the beam size at the interaction points.

Chapter 3 shows the basic tools of beam transverse dynamics, analyzes the present LHC high luminosity interaction region, identifies the limitations arising from a reduction of the beam size at the interaction points and concludes by presenting an upgrade target and two alternative options (dipole first and quadrupole first) which try to overcome different limitations.

Chapter 4 focuses on a realistic design of a dipole first upgrade layout with an analysis of the merits and challenges.

Chapter 5 focuses on realistic designs for quadrupole first layouts with an analysis of the merits and challenges. The chapter shows an original method for identifying the theoretical limitations of the quadrupole first designs and finding optimized layouts.

Chapter 6 concludes the thesis by summing up the results, comparing the presented options and introducing future plans of CERN concerning the LHC upgrade.

The appendix presents a numerical optimization algorithm implemented in an existing program for accelerator design (MADX).

## 1.2 Contributions associated with this thesis

The original work incorporated in and arising from this thesis can be organized in the following categories:

1. Original design of a dipole first option with analysis of hardware requirements, performance, limitations and correction strategies for aberrations ( [dM05], [dMBR06], [dM07b], [FGdMG07]).
2. Original designs of low gradient quadrupoles first options with analysis of hardware requirements, performance, limitations. Proposal for Phase I upgrade ( [dMB06], [BdM07], [BdMO07] ).
3. Optics design of high gradient quadrupole first options ( [KAM<sup>+</sup>07] ).
4. Development of analytical tools for final focus design ( [dM07a] ).
5. Optimization tools for optics design software and automated procedures for generating optics transitions ( [dMSS06], [SSdMF06]).

## 1.3 Acknowledgment

Thanks for the continuous support and inspiration to: Aurelio Bay, Oliver Brüning, Ulrich Dorda, Simone Gilardoni, Massimo Giovannozzi, Stéphane Fartoukh, Tom Kroyer, Frank Schmidt, Rogelio Tomas, Thys Risselada, Leonid Rivkin, Albin Wrulich.

Many thanks for the helpful discussions and ideas to: Erik Adli, Elena Benedetto, Sandro Bonacini, Chiara Bracco, Roderik Bruce, Helmut Burkhardt, Rama Calaga, Werner Herr, Jean Pierre Kouchuck, Ramesh Gubta, Etienne Forest, Andrea Franchi, Jean Bernard Jeanneret, John Johnstone, John Jowet, Emanuele Laface, Andrea Latina, Peter Limon, Daniela Macina, Nicola Mokhov, Yannis Papaphilippou, Steve Peggs, Diego Quatraro, Stefano Redaelli, Giovanni Rumolo, Guillome Robert-Demolaize, Federico Roncarolo, Benoit Salvant, Tanaji Sen, Vladimir Shiltsev, Guido Sterbini, Walter Scandale, Ezio Todesco, Frank Zimmermann.

I acknowledge the support of the European Community-Research Infrastructure Activity under the FP6 "Structuring the European Research Area" programme (CARE, contract number RII3-CT-2003-506395).

# Chapter 2

## The LHC Upgrade

### 2.1 Introduction

In this chapter I will examine the key parameter estimates for the Large Hadron Collider (LHC). An analysis of the limiting factors in the LHC performance will lead to an overview of future upgrade strategies. In the final part I will list the pros and cons of the interaction region upgrade.

### 2.2 The Large Hadron Collider

The scope of the LHC is to find experimental evidence of the Higgs mechanism which generate particle masses, gluon plasma, to perform precision measurements for validating the standard model theory and to explore new physics frontiers ([Gia99]).

The LHC is designed to fulfill this goal by colliding hadrons at unprecedented energies (14 TeV in the center of mass in proton-proton collisions and 5.52 TeV for nucleons in lead ions), and a very high luminosity (around  $10^{34} \text{ cm}^{-2} \text{ s}^{-1}$ ) which leads to around 40 proton-proton collisions in two experiments every 25 ns. Hadrons assure a large spectrum of events production because the energy of nucleons is shared between the elementary constituents (quarks and gluons).

The LHC is a synchrotron that consists of a 26.7 km ring where two counter-rotating beams collide in four interaction points (IP). The beams circulate in separate magnetic channels (they require opposite magnetic field) and are recombined before the IP. At the IP there is an experimental area equipped with particle detectors which are able to reconstruct the events occurred by tracking the fragments of the collisions (see Fig. 2.2.1). For an introduction on the machine see [BC07] and [BCL<sup>+</sup>04]. .

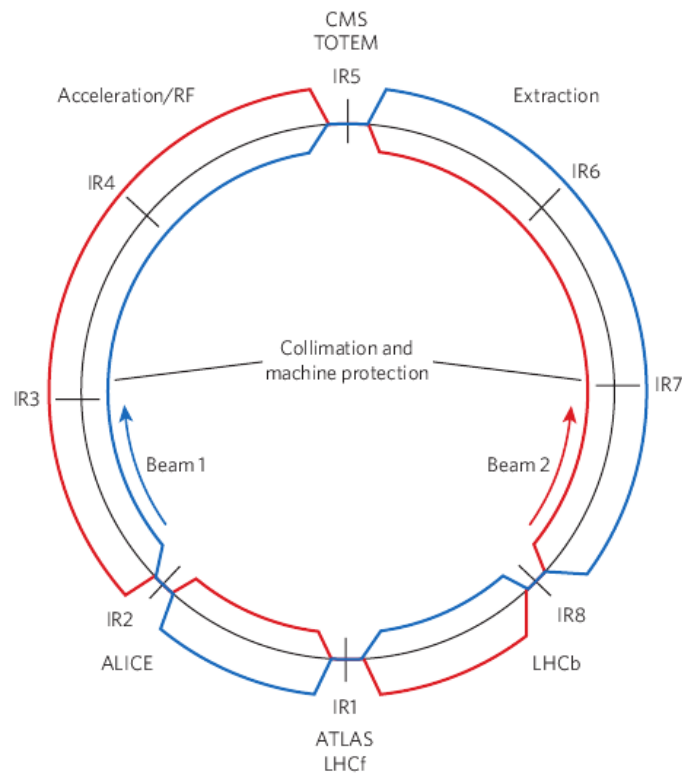


**Figure 2.2.1 LHC schematic.** LHC is composed of 8 arcs and 8 long straight sections (LSS). Two counter-rotating beams cross and collide in 4 interaction region (IR1,IR2,IR5,IR8). The other straight sections, called interaction regions (IR), are for beam collimation (IR3,IR7), RF beam acceleration (IR4) and beam dump (IR6).

In 2001 CERN launched an R&D program (see [Zim08]) to study the feasibility of an upgrade of the two key parameters, energy and luminosity (see [GMV02], [BCG<sup>+</sup>02]).

An increase of the particle energy can mainly be useful for extending the physics reach of the LHC, while an increase of the luminosity will help experiments to collect more data which translate into more accurate measurements or more chances to study rare events (like the detection of Higgs bosons decays).

An analysis of these two key parameters will identify possible upgrade scenarios.

### 2.2.1 Top energy

The maximum energy achievable by the particles in the LHC ( $E \simeq pc = 7 \text{ TeV}$ ) is limited by the radius of tunnel arcs ( $\rho = 3.5 \text{ km}$ ) and/or by the maximum bending field generated by the dipole magnets ( $B = 8.33 \text{ T}$ ). These quantities are in fact related by the equation:

$$\frac{p}{e} = f_{\text{bend}} B \rho \quad (2.2.1)$$

where  $f_{\text{bend}}$  is a factor smaller than 1 (0.8 for the LHC resulting in a maximum bending radius of 2.8 km) which takes into account the fact that the arcs cannot be completely filled by bending magnets since space must be reserved for experimental areas, stabilizing magnets, accelerating radio-frequency cavities, collimators and diagnostic components.

An increase of the energy can only be achieved by building a larger ring or by improving the magnet technology and replacing the existing magnets with new magnets that feature an increased bending field. Both of these options require enormous costs and will not be treated in this thesis.

### 2.2.2 Luminosity

The collision rate is determined by the accelerator luminosity which is a figure of merit defined by the beam parameters and accelerator lattice. It relates the cross section of an event to the event rate via the formula:

$$\frac{dR}{dt} = L\sigma \quad [L] = \text{cm}^{-2} \text{s}^{-1} \quad (2.2.2)$$

where  $R$  is the number of events and  $\sigma$  is the cross section of the event. For calculating the overall proton collision rate, the total inelastic cross section

for protons is estimated to be around 100 mb (a barn,  $b$ , correspond to  $1 \cdot 10^{-24} \text{ cm}^2$ ) and the luminosity ranges between  $1 \cdot 10^{34} \text{ cm}^{-2} \text{ s}^{-1}$  (nominal performance) and  $2.3 \cdot 10^{34} \text{ cm}^{-2} \text{ s}^{-1}$  (ultimate performance).

As the LHC is a cycled machine, the luminosity is not constant over time. The particles must first be injected in the LHC with a momentum of  $450 \text{ GeV}/c$  by the injector chain of accelerators (Source, Linac2, Booster, PS, SPS), then slowly accelerated (for about half an hour) and finally put in collision when they reach 7 TeV. At this time the luminosity will be at its peak and collision rate will be maximum. After the first collisions the beam parameters change and the luminosity decays. The processes responsible for the decay are the collisions themselves (resulting in a lifetime of 45 hours) and beam blow-up due to intra-beam scattering, rest gas collision, noise, magnetic field imperfections, long range beam beam interaction (all of them slightly compensated by the synchrotron radiation damping). The net luminosity lifetime, including all of these effects reduces to about 15 hours ([BCL<sup>+</sup>04]). When the luminosity is too low, a fresh beam is injected in order to maximize the integrated luminosity.

The integrated luminosity in fact has more physical relevance than the peak luminosity because it gives a measure of the amount of data acquired by the experiments over time. On the other hand it is more difficult to estimate due to the uncertainty involved in several processes. A discussion on the optimization of the integrated luminosity is left out from the thesis while a discussion on the peak luminosity, which can easily be estimated by the beam parameters, will be the topic of the next section.

## 2.3 Peak luminosity

The peak luminosity can be estimated (see [HM03]) from the beam parameters using:

$$L = \frac{N_b^2 f n_b}{4\pi\sigma_x^* \sigma_y^*} F(\theta_c, \sigma_x, \sigma_z), \quad (2.3.1)$$

where  $f$  is the beam revolution frequency,  $N_b$  the number of protons per bunch or bunch intensity,  $n_b$  the number of bunches,  $\sigma_x^*$ ,  $\sigma_y^*$  are the transverse RMS beam sizes at the IP,  $F$  the geometric loss factor which depends on other beam parameters (beam crossing angle  $\theta_c$ , longitudinal beam size  $\sigma_z$  and transverse beam size in the crossing plane).

This formula is valid for two Gaussian beams of equal size and if the hourglass effect is negligible (see [HM03]). The hourglass effect, which in our

Name	Symbol	Values
Revolution frequency	$f$	11245 kHz
Protons per bunch	$N_b$	$1.15 \cdot 10^{11}$
Number of bunches	$n_b$	2808
Transverse RMS beam size	$\sigma_x$	16.6 $\mu\text{m}$
Crossing angle	$\theta_c$	296 $\mu\text{rad}$
Longitudinal RMS beam size	$\sigma_z$	7.5 cm
Geometric loss factor	$F$	0.829757

**Table 2.1** Nominal parameters of the LHC.

context is negligible, will be discussed in Sec. 2.3.4.

The nominal LHC parameters are given in table 2.1. The implications of these quantities for an LHC upgrade will be explained in the following sections.

### 2.3.1 Bunch intensity

As the LHC is optimized for reaching the highest luminosity, the first target is to increase the number of proton per bunches ( $N_b$  or ppb) because this quantity increases the luminosity quadratically. This is the main reason why the LHC is a proton-proton collider and not a proton anti-proton collider because it is very difficult to produce highly populated anti-proton bunches. On the other hand high bunch intensity is difficult to achieve because of several limitations.

A first limitation comes from the beam beam interactions in and close to the interaction points. The electromagnetic field of one beam, proportional to its charge, distorts the dynamics of the other beam resulting in a growth of the beam size which limits the luminosity and generate beam losses that may quench the superconducting magnets. The beam beam effect can not be evaluated exactly but can be quantified by a quantity,  $\Delta Q_{\text{ho}}$ , obtained by measuring the linear effect on the beam dynamics. The value for  $\Delta Q_{\text{ho}}$  is:

$$\Delta Q_{\text{ho}} = \frac{N_b r_p}{4\pi \varepsilon_n}, \quad (2.3.2)$$

where  $r_p$  is the classical proton radius  $r_p = q_e^2 / (4\varepsilon_0 m_p c^2) \simeq 1.53 \cdot 10^{-18}$  m and  $\varepsilon_n = 6.75$  mrad m is the normalized emittance (see Eq. 3.2.24 in Sec. 3.2.2 for the exact definition of this quantity). Experience with existing hadron collider machines indicates that the total linear tune shift (sum of all IP's) should not exceed 0.015 to assure beam stability. For the LHC the nominal

intensity  $N_b = 1 \cdot 10^{11}$  yields  $\Delta Q_{\text{ho}} = 0.0032$  per IP, while the ultimate intensity is defined for  $N_b = 2.3 \cdot 10^{11}$  which is at the limit for the beam beam tune shift.

The beams continue to interact nearby the interaction region for the reason discussed in Sec. 2.3.4 and 3.4.3. This type of interactions are called long range beam beam interactions (LRBB interactions). The LRBB interactions present similar limitations to the head-on beam beam interaction and their effects depend again on the bunch intensity (see [CT99]).

The bunch intensity enters in the definition of the beam current which is responsible to another set of limitations that will be discussed in Sec. 2.3.2.

The effects mentioned above show that boosting the luminosity by an increase of the bunch intensity is a delicate issue because it affects a large number of machine subsystems. As an upgrade project, the increase of the bunch intensity has a large potential but also a large uncertainty.

### 2.3.2 Number of bunches

The bunch intensity, together with the number of bunches  $n_b$ , define the value of the beam current:

$$I_b = N_b n_b f q. \quad (2.3.3)$$

The number of bunches depends on the bunch spacing and filling factor. It affects the multi-bunch instabilities, the heat load in the cryogenic system, the beam stored energy (350 MJ at a particle energy of 7 TeV and nominal intensity) and, in addition, the number of long range beam beam interactions.

The multi-bunch instabilities arise from the electromagnetic wake fields in the beam pipe interacting with beam (see [Cha93]).

As the bunch pass through the beam pipe, it creates also image currents which are proportional to the beam current. They deposite heat close the superconductors triggering a quench if the cryogenic system does not remove the heat.

In addition, the bunch charge stimulates electron emission and the build up of an electron cloud. This in turn genetates additional heat and causes beam instabilities.

As the LHC is a superconducting machine, all the heat must be extracted at cryogenic temperatures (1.8 K) by the cryogenic system which is already at limits of its heat transfer capabilities or cooling power.

On top of this the stored beam energy is proportional to the bunch current. A large stored beam energy creates hazard to the equipments and require sophisticated protection mechanisms.

A decrease of the bunch spacing, which would be required to increase the number of bunches, will increase the number of the long range beam beam interaction as it will be discussed in Sec. 2.3.4.

In conclusion, an increase of the number of bunches show similar drawbacks of an increase of the bunch intensity but the increase of luminosity is only linear.

### 2.3.3 Transverse beam size at the IP

If we neglect the geometric reduction factor, the inverse of the transverse beam size (or beam cross section) at the IP gives a linear increase of the luminosity. It is a local quantity that affects a limited part of the accelerator, if we exclude the aberrations of the beam that tend to increase as the beam size diminishes. These facts make it a good candidate for an upgrade project because a limited intervention is able to boost the performance without affecting the rest of the machine. The upgrade of the interaction region is the main topic of this thesis.

The beam size at the IP is determined by the focusing properties of the quadrupole magnets and the layout of the long straight section (LSS) which connects the ring arcs and hosts the experiments. The fact that the quadrupole strength of the magnets and the total length of the LSS are limited, poses a limit on the minimum beam size achievable in the LHC. In addition, another limits comes from the geometric reduction factor which starts to play a role in the luminosity estimation when the transverse beam size is small compared to the longitudinal one, as we will see in Sec. 2.3.4.

### 2.3.4 Geometric reduction factor

The geometric reduction factor enters in the luminosity estimation (Eq. 2.3.1) when the beams collide with a crossing angle. When the bunches collide with a crossing angle the effective area of interaction is reduced and the luminosity as well (see fig 2.3.2) .

The geometric reduction factor can be computed using:

$$F = \frac{1}{\sqrt{1 + \left(\frac{\theta_c \sigma_z}{2\sigma_x^*}\right)^2}}, \quad (2.3.4)$$

where  $\theta_c$  is the crossing angle,  $\sigma_z$  is the longitudinal beam size,  $\sigma_x^*$  is the transverse beam size in the crossing plane.

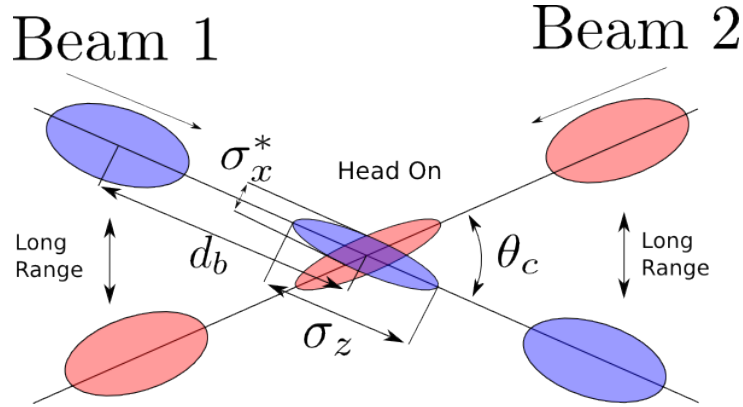


**Figure 2.3.2** Collision of the LHC beams.  $\theta_c$  is the crossing angle. The larger is the crossing angle, the smaller is the area of overlap and therefore the smaller is the luminosity. It is worth noting that while  $\sigma_z$  is constant over the machine,  $\sigma_x$  varies and assumes its minimum in the IPs.

This is an approximation of a more complex formula (see [HM03] ) that takes into account the hourglass effect, that is fact that the transverse beam size at the IP is not constant but increases with the distance from the IP. In our context this effect is negligible because in case of a crossing angle the beams overlap only in a small region where the transverse beam size is almost constant.

If the two bunched beams are in close contact in the same region like in the detector, their trajectory need to be separated by a certain angle in order to avoid parasitic collision, therefore a crossing angle is needed. As we will see in Sec. 3.3.1 Eq. 3.3.5, the crossing angle  $\theta_c$  should be taken proportional to  $1/\sigma_x$  in order to keep the effect of the long range interactions under control, therefore:

$$F \sim 1 \quad \text{for } \sigma_x \gg \theta_c \sigma_z \quad (2.3.5)$$

$$F \sim \sigma_x^2 \quad \text{for } \sigma_x \ll \theta_c \sigma_z. \quad (2.3.6)$$

Equation 2.3.6, substituted in the equation for the luminosity (Eq. 2.3.1), implies that the luminosity will saturate at a certain value when the beam size is reduced in case of round beams (see the black curve in Fig. 2.3.3). For the LHC the beam is round at the IP and transverse RMS beam size is about  $17 \mu\text{m}$ .

In case of elliptic beam ( $\sigma_x \neq \sigma_y$ ), the  $\sigma$  in the crossing plane can be fixed, while the  $\sigma$  in the other plane can be reduced as much as possible without luminosity losses (see Fig. 2.3.3 ).

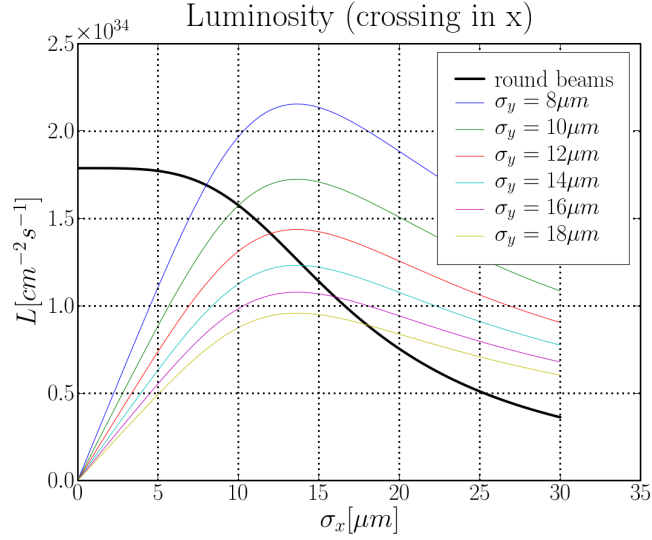


**Figure 2.3.3** Luminosity gain depending on  $\sigma_x$  and  $\sigma_y$ . The curves are calculated using the nominal beam parameters. The crossing angle in the  $x$  plane is chosen to keep the separation of the two beam at  $9.8\sigma$ . The thick line shows the luminosity for round beams, while the other lines show the luminosity when  $\sigma$  in the non crossing plane ( $y$ ) is varied.

For a given beam cross section the luminosity can be increased by using elliptic beams. For hadron machines and in particular for proton proton machines it is less straightforward to generate flat beams compared to leptons or proton anti-proton colliders as we will see in Sec. 5.3.

In the regime of small bunch sizes, reducing the bunch length is beneficial as shown in Fig. 2.3.4.

It is possible to overcome the limitations of the geometric reduction factor by several means: crab crossing, early separation and wire compensation.

Crab cavities (see [Ohm05], [Tüc07], [CTZ07] and [TdMZ07]) create an oscillation in the crossing plane such that the two beams, while having a crossing angle, will collide head on with an exact superposition.

The early separation scheme (see [KAM<sup>+</sup>07]) aims to separate the two beams as soon as possible in order to reduce the beam beam encounters and implies a modification of the detector area.

Wire compensation (see [Zim05] and [DZ07]) and electron lens (see [DZFS]) aim at a reduction of the effects of the beam beam interaction allowing more beam current or smaller crossing angle and constant luminosity

The discussion of these approaches is beyond the the scope of this thesis.

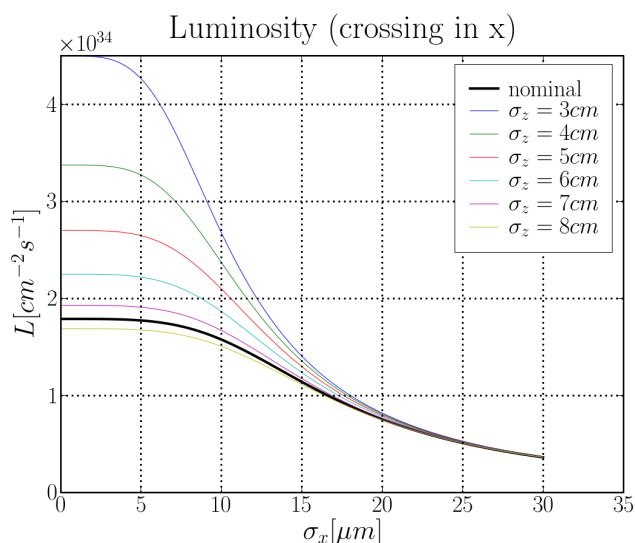


**Figure 2.3.4** Luminosity gain for round beams depending on  $\sigma_x = \sigma_y$  and  $\sigma_z$ . The thick curve represents the nominal parameters. A reduction of  $\sigma_z$  is more beneficial at small  $\sigma_x$ .

## 2.4 Conclusion

I gave a survey of the key parameters of the LHC: top energy and luminosity. An analysis of the limiting factors allowed to identify several upgrade strategies for upgrading the top energy:

- building a new tunnel and additional magnets,
- improve magnet technology and replace all the magnets

and for upgrading the peak luminosity:

- increase bunch intensity
- increase number of bunches
- reduce the transverse beam size at the IP
- reduce the effect of the geometric reduction factor

In the rest of the thesis I will focus on the upgrade strategy that aims at a reduction of the transverse beam size. This option has the clear advantage of requiring a localized upgrade in the two insertion. It will be shown that the upgrade of the interaction region has a realistic potential to increase the

luminosity by a factor from 1.4 to 2 with respect to the nominal luminosity. In order to achieve larger improvement an upgrade of the interaction region must be coupled with other upgrade options.

In the following chapter I will describe and discuss the limitations of the nominal interaction region layout. The chapter concludes with the introduction of two upgrade options that will be discussed in detail in the rest of the thesis.



# Chapter 3

## LHC interaction region layout

### 3.1 Introduction

In this chapter I introduce the basic concepts that are needed to study the beam dynamics in the accelerators. A discussion on the issue of reducing the beam size at the IP will lead to description of the LHC interaction region layout. The layout will be analyzed and its limitations discussed. In the conclusion I identify two possible upgrade path that will be analyzed in the following chapters.

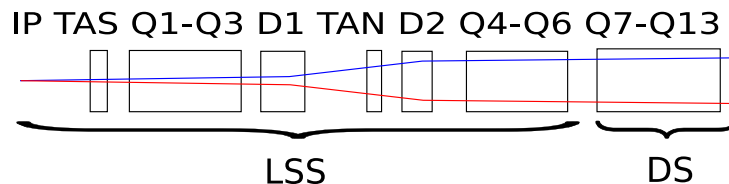


Figure 3.1.1 LHC interaction region (IR) schematic. Blue and red lines are the trajectories of Beam 1 and Beam 2 respectively.

### 3.2 Beam dynamics

In accelerators the dynamics of a beam of charged particles is governed mainly by the classical effect of the electromagnetic fields (quantum effects are involved during collisions and in the presence of strong synchrotron radiation).

The electromagnetic fields act on the particles via the Lorentz force:

$$\frac{d\mathbf{p}}{dt} = q(\mathbf{E}(\mathbf{r}) + \mathbf{v} \times \mathbf{B}(\mathbf{r})) \quad (3.2.1)$$

where  $\mathbf{p}$ ,  $\mathbf{v}$ ,  $\mathbf{r}$  and  $q$  are the momentum, velocity, position and charge of a particle and  $\mathbf{E}(\mathbf{r})$ ,  $\mathbf{B}(\mathbf{r})$  is the electromagnetic field at the instantaneous position of the particle. The form of the Lorentz force shows that for relativistic particles the energy can be modified using electric field and the direction is efficiently changed using magnetic fields.

Electromagnetic fields are often generated in a vacuum chamber using magnets and RF cavities (sometimes a plasma is used as source of EM fields). In case of the LHC a large number of dipole magnets generate a uniform transverse magnetic field which guides the beam in a circular trajectory, a small set of RF cavities provides acceleration and stability for the longitudinal (along the circular trajectory) motion, a large set of quadrupole magnets provide transverse (perpendicular to the circular trajectory) stability and another large set of smaller dipole, quadrupole, multipole corrector magnets provide additional stability by correcting natural aberrations and imperfections.

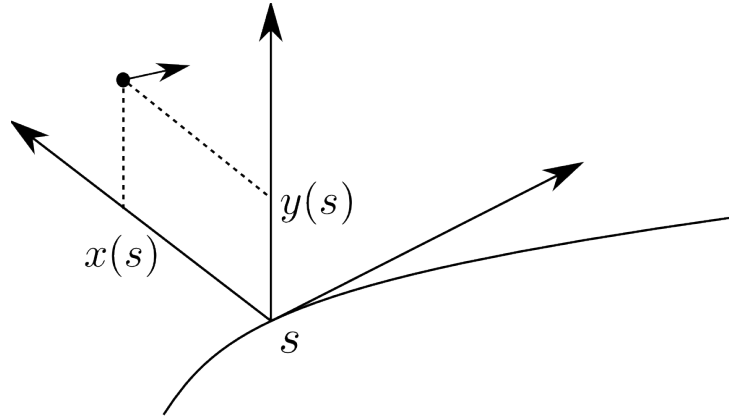


**Figure 3.2.2** Moving coordinate system for accelerators.

In accelerators like the LHC a moving coordinate system is often used (see Fig 3.2.2): a reference particle identifies a reference trajectory and the actual trajectory of any particle is specified by the path length position  $s$ , the transverse coordinate  $x, y$  of the plane orthogonal to the trajectory in  $s$  and the path length difference  $-ct$  between the actual particle and the reference particle. In this reference frame the coordinate  $s$  acts as a time parameter and the motion has 3 degrees of freedom  $x, y, -ct$ . For the LHC the reference trajectory lies in the horizontal plane indicated by the coordinate  $x$ .

For the LHC and in general for large storage rings, the motion in different planes can be decoupled in a first approximation. This allows to study separately the motion in the transverse planes and the one in the longitudinal

plane. This thesis will be mostly focused on the transverse dynamics (i.e. the motion in the transverse plane) because it allows to study the beam size at the IP.

### 3.2.1 Transverse dynamics

In the LHC, the force acting in the transverse plane is determined mostly by the transverse magnetic field of the magnets. The equations of motion of a particle due to a magnetic field  $(B_y, B_x)$  in the transverse plane and in a straight reference system can be approximated by:

$$x''(s) = -\frac{q}{p} \frac{1}{1 + \delta} B_y(s) \quad (3.2.2)$$

$$y''(s) = +\frac{q}{p} \frac{1}{1 + \delta} B_x(s), \quad (3.2.3)$$

where the prime is referred to a derivative with respect to  $s$ ,  $q$  is the charge of the particle,  $p$  is the momentum of the reference particle,  $p(1 + \delta)$  is momentum of the particle and  $\delta$  the deviation of the momentum from the reference momentum  $p$ . The approximation used, called paraxial approximation, assume that  $x' \simeq p_x/p$  and neglects the fact that the total momentum depends on the transverse momenta.

A bi-dimensional source free magnetic field can conveniently be expanded in:

$$B_y + iB_x = \sum_{n=0} (B_{n+1} + iA_{n+1}) \left( \frac{x + iy}{r_0} \right)^n, \quad (3.2.4)$$

where  $r_0$  is a reference radius and the terms  $B_{n+1}$ ,  $A_{n+1}$  are called field multipole components that can be measured with rotating coils and computed with numerical codes.

It is possible to define pure geometrical quantities called normalized strengths, normalized with the particle reference momentum  $p$ , using:

$$k_n = \frac{q}{p} \frac{\partial^n B_y}{\partial x^n} = \frac{q}{p} \frac{n!}{r_0^n} B_{n+1} \quad B_{n+1} = \frac{r_0^n}{n!} \frac{\partial^n B_y}{\partial x^n} \quad (3.2.5)$$

$$\hat{k}_n = \frac{q}{p} \frac{\partial^n B_x}{\partial x^n} = \frac{q}{p} \frac{n!}{r_0^n} A_{n+1} \quad A_{n+1} = \frac{r_0^n}{n!} \frac{\partial^n B_x}{\partial x^n} \quad (3.2.6)$$

where  $k_n$  are called normal components and  $\hat{k}_n$  are called skew components.

The equation of motion can be written as:

$$x''(s) = -\text{Re} \left[ \sum_{n=0} \frac{k_n(s) + i\hat{k}_n(s)}{1 + \delta} \frac{(x(s) + iy(s))^n}{n!} \right] \quad (3.2.7)$$

$$y''(s) = \text{Im} \left[ \sum_{n=0} \frac{k_n(s) + i\hat{k}_n(s)}{1 + \delta} \frac{(x(s) + iy(s))^n}{n!} \right] \quad (3.2.8)$$

In case of a curved reference trajectory, the equation of motion becomes

$$x''(s) + \frac{q}{p} B_1(s) h_x(s) x(s) + h_x(s) = -\frac{q}{p} \frac{1}{1 + \delta} B_y(s) \quad (3.2.9)$$

$$y''(s) + \frac{q}{p} A_1(s) h_y(s) y(s) + h_y(s) = +\frac{q}{p} \frac{1}{1 + \delta} B_x(s), \quad (3.2.10)$$

where  $h_x(s), h_y(s)$  are the inverse of the local radius of curvature. Usually the bending magnets generate the curvature and in case there is no field error  $\frac{q}{p} B_1(s) = h_x(s)$  and  $\frac{q}{p} A_1(s) = h_y(s)$ .

### 3.2.2 Linear dynamics

The LHC, like large storage rings, is designed to have a quasi linear motion. The sources of non linear magnetic fields are kept as small as possible, unless they are used to compensate natural aberrations (chromatic sextupoles) or provide additional stability (Landau octupoles). It is therefore possible to study the linear dynamics in a first approximation and treat the non linear terms as a perturbation.

#### Hill equation

In a linear approximation and assuming no first order coupling ( $\hat{k}_1 = 0$  and  $k_0 = 0$ ), the equation of motion (Eq. 3.2.7) have the form:

$$z''(s) + k(s)z = g(s), \quad (3.2.11)$$

where  $z$  now refers to both transverse coordinates  $x$  and  $y$ ,  $k(s) = k_1 + k_0 h_x$  for the  $x$  plane and  $k(s) = -k_1$  for the  $y$  plane and  $g(s) = k_0 - h_x$ .

#### Periodic solution and $\beta$ function

Equation 3.2.11, called Hill equation, has an important feature for circular machine:  $k(s)$  is a periodic function of  $s$  of period  $L$ , where  $L$  is total path

length. This allows the use of the Floquet theory and an elegant formalism due to Courant-Snyder [CS58] can be used to describe the linear uncoupled motion.

The first consequence of the periodicity for the Hill equation is that it is possible to write the solution of the homogeneous equation of motion

$$z''(s) + k(s)z = 0 \quad (3.2.12)$$

as:

$$z(s) = \sqrt{2I\beta(s)} \cos(\phi(s) + \psi), \quad (3.2.13)$$

where  $I$  and  $\psi$  is the action and initial phase of the particle and  $\beta(s)$  and  $\phi(s)$  are periodic functions which depend only on  $k(s)$ . In fact they follow the equations:

$$\frac{1}{2}\beta(s)''\beta(s) - \frac{1}{4}\beta(s)'^2 + k(s)\beta(s)^2 = 1 \quad (3.2.14)$$

$$\phi(s) = \int_{s_0}^s \frac{1}{\beta(t)} dt \quad (3.2.15)$$

These equations can be put in another form, defining  $w(s) = \sqrt{\beta(s)}$ :

$$\phi' = \frac{1}{w^2} \quad w'' - \frac{1}{w^3} + kw = 0, \quad (3.2.16)$$

which will be very useful for the design of the interaction region layout, as we will see in Sec. 5.3.

## Tune

The tune  $Q$  is defined as:

$$Q = \frac{1}{2\pi} \int_{s_0}^L \phi(t) dt = \frac{1}{2\pi} \int_{s_0}^L \frac{1}{\beta(t)} dt, \quad (3.2.17)$$

where  $L$  is the length of the accelerator.

It represents the number of oscillations (called betatron oscillations) that a particle makes in the transverse plane in one turn. The fractional part of the tune is extremely important for the stability of the motion, as we will see later.

### Closed orbit

In case the factor  $g(s) = k_0 - h(s)$  in the Hill equation 3.2.11, the closed orbit is defined as the periodic trajectory of the inhomogeneous Hill equation. It is given by:

$$x_{\text{co}}(s) = \frac{\sqrt{\beta(s)}}{2 \sin(\pi Q)} \int_s^{s+L} g(t) \sqrt{\beta(t)} \cos(|\phi(t) - \phi(s)| - \pi Q) dt. \quad (3.2.18)$$

The term  $g(s)$  is determined by orbit correctors, dipole errors or misalignments of high order multipoles. The closed orbit can be defined also as the average trajectory of many particles.

### Twiss parameters

The first derivative  $z'(s)$  can be conveniently expressed as:

$$z'(s) = \sqrt{\frac{2I}{\beta(s)}} \left( \alpha(s) \cos(\phi(s) + \psi) + \sin(\phi(s) + \psi) \right) \quad (3.2.19)$$

$$z'(s) = \sqrt{2I\gamma(s)} \cos(\chi(s) + \psi) \quad (3.2.20)$$

$$\tan(\phi(s) - \chi(s)) = \frac{1}{\alpha(s)}, \quad (3.2.21)$$

by defining the periodic quantity:

$$\alpha(s) = -\frac{1}{2}\beta'(s) \quad \gamma(s) = \frac{1 + \alpha(s)^2}{\beta(s)} \quad (3.2.22)$$

The quantities  $\alpha, \beta, \gamma$  are called Twiss parameter and are used for describing the linear uncoupled motion. It possible to show that the action  $I$  is an invariant of the motion (called Courant-Snyder invariant) because:

$$\gamma(s)z(s)^2 + 2\alpha(s)z(s)z'(s) + \beta(s)z'(s)^2 = 2I. \quad (3.2.23)$$

$I$  is proportional to the area of the phase space ellipse described by Eq. 3.2.23.

If we assume that the particles have a Gaussian distribution in the action and an uniform uncorrelated distribution on the initial phase it is possible to show also that:

$$\varepsilon = \sqrt{\langle z^2 \rangle \langle z'^2 \rangle - \langle zz' \rangle^2} \quad (3.2.24)$$

$$\langle z^2 \rangle = \beta\varepsilon = \sigma^2 \quad (3.2.25)$$

$$\langle zz' \rangle = -\alpha\varepsilon \quad (3.2.26)$$

$$\langle z'^2 \rangle = \gamma\varepsilon, \quad (3.2.27)$$

where  $\varepsilon$ , called beam emittance, is a statistical quantity which indicates the size of the ellipse which encloses the phase space distribution of a given fraction of particles. The Twiss parameters have a direct interpretation as measurable quantities.

Under a linear motion it is possible to show that  $\varepsilon = \langle I \rangle$  and the emittance is conserved. If the system is non linear, while the volume of the phase space distribution of an ensemble of particles is conserved (at the action as well), the emittance change with time because the phase space distribution get distorted and the ellipse that encloses the phase space distribution of a given fraction of particles changes volume.

During acceleration the emittance shrinks as a consequence of the adiabatic damping. When the longitudinal momentum is increased, the transverse one remains constant and therefore the absolute values of the divergence ( $|x'| \simeq |p_x|/p$ ). As a consequence the action of the particles and therefore the emittance reduces as well. The net effect is that the so called normalized emittance, defined by:

$$\varepsilon_n = \frac{\varepsilon}{\gamma_r}, \quad (3.2.28)$$

where  $\gamma_r$  is the relativistic gamma factor, is conserved during acceleration.

### 3.2.3 Non linear perturbations

In case of non-linear terms are present, the motion is no longer analytically solvable and a perturbation approach is used to estimate the effects of the non-linear terms on the linear dynamics.

Using a simple approach it is possible to show the effect of a non linear perturbation. We assume that the turn by turn unperturbed motion is given by:

$$x_0(s, m) = \text{Re} \left( A_x w_x(s) e^{i(\phi_x(s \bmod L) + 2\pi m Q_x)} \right) \quad (3.2.29)$$

$$y_0(s, m) = \text{Re} \left( A_y w_y(s) e^{i(\phi_y(s \bmod L) + 2\pi m Q_y)} \right), \quad (3.2.30)$$

where in  $A_x, A_y$  there are the initial amplitude and phase in complex coordinates,  $L$  is the period and  $m$  represents the number of turns.

Using Eq. 3.2.7, a deflection  $\Delta x', \Delta y'$  from a localized perturbation at a given  $s_0$  and a given turn  $m$  will be given by:

$$\Delta x'(s_0) = -\Delta s \operatorname{Re} \left( (k_n(s_0) + i\hat{k}_n(s_0)) \frac{(x_0(s_0) + iy_0(s_0))^n}{n!} \right) \quad (3.2.31)$$

$$\Delta y'(s_0) = \Delta s \operatorname{Im} \left( (k_n(s_0) + i\hat{k}_n(s_0)) \frac{(x_0(s_0) + iy_0(s_0))^n}{n!} \right), \quad (3.2.32)$$

where we assume that a small perturbation ( $k_n + i\hat{k}_n$ ) in  $s_0$  for a small  $\Delta s$ .

As a consequence of Eq. 3.2.13, the deflection will result in a displacement at the location  $s_1$  in the  $x$  plane:

$$\Delta x(s_1) = \Delta x'(s_0) w_x(s_1) w_x(s_0) \sin(\phi_x(s_1) + 2\pi m Q_x) \quad (3.2.33)$$

$$= \Delta x'(s_0) w_x(s_1) w_x(s_0) \operatorname{Re} \left( e^{i(\phi_x(s_1) + \frac{\pi}{2} + 2\pi m Q_x)} \right) \quad (3.2.34)$$

Using Eq. 3.2.29, 3.2.31 and 3.2.33, for a given  $k_n$  in  $\Delta x(s')$  there will be terms of the type:

$$\frac{k_n}{n!} x_0^p (iy_0)^q = \frac{k_n}{n!} w_x^{(p+1)} w_y^q e^{i((p+1)(\phi_x + \frac{\pi}{2}) + q(\phi_y + \frac{\pi}{2}))} e^{i2\pi m((p+1)Q_x + qQ_y)} \quad (3.2.35)$$

being  $p, q$  given integers depending on  $n$ .

The arguments in the exponential in Eq. 3.2.35 show that when  $(p+1)Q_x + qQ_y$  for the  $x$  plane or  $pQ_x + (q+1)Q_y$  for the  $y$  plane are close to an integer, the kicks vary slowly turn after turn, resulting in resonant excitation of the particle. The couple  $(p+1, q)$  are called resonances and defines lines in the  $Q_x, Q_y$  diagram (see Fig. 3.2.3). If the tunes are close to one of this line, the machine exhibit a resonant behavior which is driven by the set of multipoles responsible of the resonant terms.

The terms that multiply the exponential in Eq. 3.2.35 also show that non linear fields are dangerous at the location where  $w = \sqrt{\beta}$  are large and that low order multipoles have larger effects than high order ones. In Sec. 3.4.2 and Sec. 3.4.6 we will see the implication of resonances in the design of the interaction region.

### 3.2.4 Dispersion and chromatic effects

So far we have considered a monochromatic beam (all the particle with the same total momentum). In reality the beam has a certain spread of energy, typically in the order of  $1 \cdot 10^{-4}$ . For an off momentum particle the closed orbit is not anymore the one of the on momentum particles. In order to study the dynamics around the on momentum closed orbit we have to modify the equations of motion. They become in a first approximation:

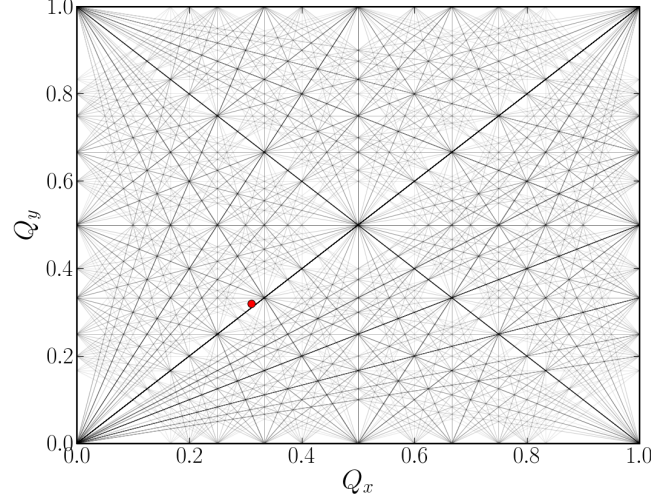


**Figure 3.2.3** Resonance lines driven by multipole up 6th order (dodecapole). The point shows the LHC working point.

$$x''(s) + k(s)x(s) = k_0(s)\delta \quad (3.2.36)$$

where  $\delta = \Delta p/p$  is the variation of the energy. From this equation it is possible to compute the so-called dispersion which is:

$$D_x = \frac{\partial x}{\partial \delta}. \quad (3.2.37)$$

The dispersion can be interpreted as the linear shift of the closed orbit for an off momentum particles. In the LHC the dispersion is generated mainly by the main bending magnets, orbit correctors and field imperfections.

An important effect, called chromaticity, that is not taken into account in Eq. (3.2.36) is the change of the focusing strength with  $\delta$ . The normalized quadrupole strength in the equation of motion must be replaced by:

$$k_1 \frac{1}{1 + \delta} \simeq k_1(1 - \delta + \delta^2 - \dots). \quad (3.2.38)$$

The effect on the transverse motion is a decrease of the tune and a generation of beating wave for the beta function called off momentum beta-beat.

These two effects can be quantified by the terms:

$$Q = Q_0 + Q_1\delta + \frac{Q_2}{2}\delta^2 + \dots \quad (3.2.39)$$

$$\beta(s) = \beta_0(s) + \beta_1(s)\delta + \frac{\beta_2(s)}{2}\delta^2 + \dots, \quad (3.2.40)$$

where

$$Q_1 = -\frac{1}{4\pi} \oint_{\text{ring}} k(s)\beta_0(s)ds \quad (3.2.41)$$

$$\beta_1(s) = -\oint_{\text{ring}} k(s)\beta_0(s) \cos(2|\phi'_0(s) - \phi(s')| - 2\pi Q_0)ds' \quad (3.2.42)$$

$$Q_2 = -\frac{1}{4\pi} \oint_{\text{ring}} k(s)\beta_1(s)ds. \quad (3.2.43)$$

The chromaticity can be corrected using sextupole magnets in a region with non zero dispersion. A sextupole can be seen as a quadrupole whose strength depends linearly on the transverse offset. A region with dispersion has a transverse offset which is proportional to the energy deviation and therefore a sextupole can be used to compensate the chromatic effect coming from the quadrupoles.

Figure 3.2.4 shows the chromatic change of the tune for the LHC when the first order is corrected by the arc sextupoles.

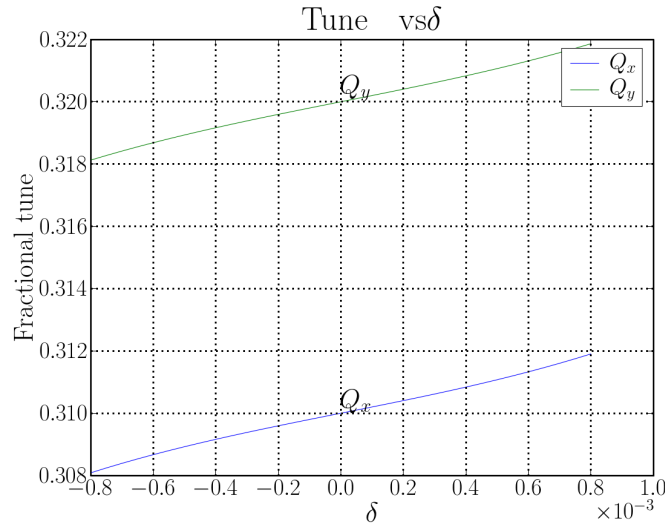


**Figure 3.2.4 Chromatic change of the tune after linear correction for the LHC.**

The chromatic effects are critical for the upgrade layout as will be explained in Sec. 3.4.6, 4.7 and 5.7.

### 3.3 Interaction region layout

We now use the concepts introduced to study the transverse beam size in the interaction region.

#### 3.3.1 Detector area

As we discussed in Sec. 2.3.3 the LHC aims at an RMS beam size of around  $17\ \mu\text{m}$  at the two high luminosity insertion which translates in  $\beta^* = 55\ \text{cm}$ .

The region around the interaction point is occupied by particle detectors. In the LHC they extend to about  $\pm 19.5\ \text{m}$  around the IP. The magnetic field inside the detector is longitudinal and it has a marginal effect on the transverse dynamics. The region can be seen as a field free region where  $k_1 = 0$ . This allows to find the corresponding beam size in the area by solving Eq. (3.2.14) for  $k_1 = 0$ . Starting from the initial condition at the IP:

$$\beta(0) = \beta^* \quad (3.3.1)$$

$$\beta'(0) = -2\alpha(0) = 0 \quad (3.3.2)$$

$$\gamma(0) = 1/\beta^*, \quad (3.3.3)$$

we find a quadratic growth of the beta function:

$$\beta(s) = \beta^* + \frac{s^2}{\beta^*} \quad (3.3.4)$$

At the end of the detector it implies  $\beta = 688\ \text{m}$  and  $\sigma = 588\ \mu\text{m}$ .

In the LHC the bunch spacing is  $25\ \text{ns}$ , therefore every  $7.5/2\ \text{m}$  the two counter rotating beams occupy the same longitudinal position. Therefore a crossing angle is needed to separate them in order to avoid parasitic collisions. Experiences with existing colliders show that a safe separation should be larger than  $10\sigma$ . Using Eq. 3.3.4 it is possible to find the crossing angle  $\theta_c$  as a function of the separation  $d_{\text{sep}}$  in  $\sigma$ :

$$\theta_c = d_{\text{sep}} \sqrt{\frac{\varepsilon}{\beta^*}} = d_{\text{sep}} \frac{\varepsilon}{\sigma^*} \quad (3.3.5)$$

For the LHC the crossing angle is about  $300\ \text{mrad}$ .

While the core of the beam extend to about  $\pm 3\sigma$ , the beam should be also safely far from the wall of the vacuum chamber for reducing the beam losses and the impedance effects. It should be assumed that the center of the beam be at least  $10\sigma$  away from the walls of the vacuum chamber.

In total the beam needs a vacuum chamber of at least  $30\sigma$  wide if two beams are present or  $20\sigma$  in case of a single beam (see Fig. 3.3.5). At the end of the detector the two beams occupy a transverse size of  $18\ \text{mm}$ .

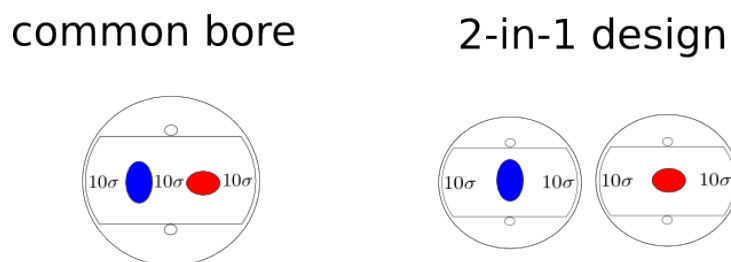


**Figure 3.3.5** Mechanical aperture required by the beam for single bore like in the LHC magnets near the IP and 2-in-1 magnets like the magnets in the LHC arcs.

### 3.3.2 TAS

A absorber called TAS (Target Absorber Secondaries) is placed immediately after the detector in order to shield the downstream magnets from the secondary particles (debris or fragments) produced by the collisions at the IP. It is a 1.8 m long copper cylinder with 34 mm aperture diameter which finishes at 23 m from the IP. At this location the beam size grows up to 21 mm for a  $\beta = 1$  km.

### 3.3.3 IR Triplets

In order to avoid an excessive growth of the beam size a compact focusing system is placed around the detectors in the LHC. The focusing system uses a set of three quadrupoles arranged in the so-called triplet structure (see Fig. blue boxes in 3.3.6), that is, three quadrupoles, named Q1, Q2 (split in two modules) and Q3, with alternating polarity.

For instance in IR5, the first quadrupole on the right of the IP has a positive  $k_1$  for Beam 1 which means focusing in the  $x$  plane and defocusing for the  $y$  plane. Beam 2 sees the same field, but because it has opposite momentum, the effect is opposite, that is defocusing in the  $x$  plane and focusing in the  $y$  plane.

The nominal LHC IR layout is called quadrupole first because of the presence of a triplet just after the detector. As we will see later in Sec.3.5 and Ch. 4 another strategy can be applied.

The effect of the triplet is to change the sign of the slope of the beta function in order to focus the beam. A side effect, due to the alternating focusing, is that the beta function and therefore the beam size grows substantially inside the triplet before being focused. For the LHC the beam size grows up 45 mm for a  $\beta = 4.5$  km. The increase of the beta function

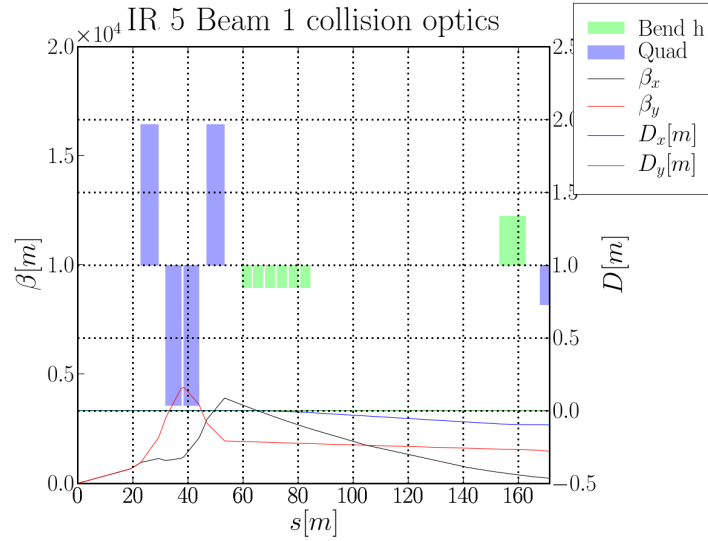


**Figure 3.3.6** LHC IR 5 optics functions in a region close to the IP. The boxes represent the position, length and polarity of the quadrupoles (blue) and dipoles (green). The pictures show the triplets Q1-Q3, the separation/recombination dipoles D1-D2 and the first quadrupole of the matching section Q4.

in the triplet is unavoidable and depends mainly on the integrated absolute gradient of the quadrupoles. A detailed analysis is given in sec. 5.3.

The triplet magnets have a large aperture of 70 mm, unfortunately the aperture of the quadrupoles cannot be fully used to accommodate the vacuum chamber. The aperture usually refers to the inner coil diameter. The first item to be put inside the aperture is the beam pipe. The beam pipe (or cold bore) is a stainless tube (1.8 mm thick) that must satisfy the requirements related to the pressure vessel code. This implies that the tube wall must have a minimal thickness to sustain the load of 25 bar. The clearance between the coils and the beam pipe is 1.75 mm and it is filled by liquid Helium for cooling purposes. In the beam pipe it is necessary to introduce a beam screen to protect the cold bore from synchrotron radiation and ion bombardment. The beam screen is a stainless steel perforated tube with a rectellipse shape (see Fig. 3.3.7).

The beam screen thickness is 1 mm plus 0.7 mm for the support ring and 0.7 mm of clearance. The beam screen has an inner layer of copper (50  $\mu\text{m}$ ) which reduces the impedance, but it creates mechanical stresses in case of quench due to the eddy currents. There is 1 mm of uncertainty in the position of the beam screen. In addition the inner most quadrupole in the triplet has

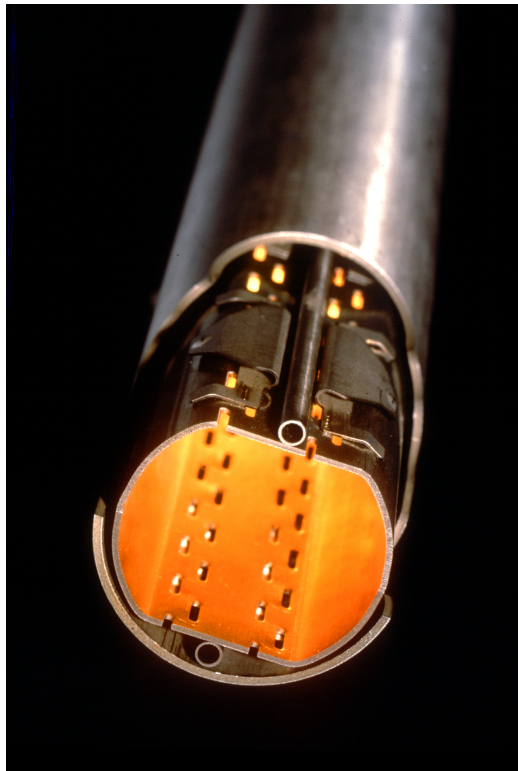
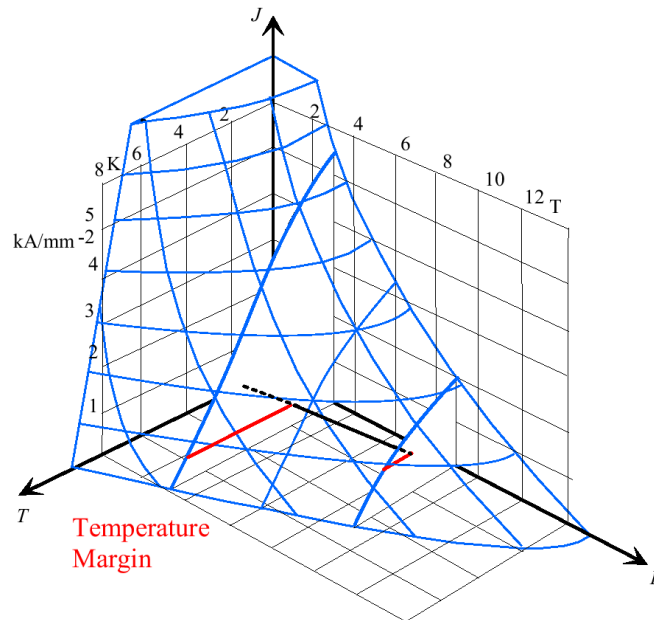


Figure 3.3.7 LHC beam pipe and beam screen with the supporting ring.

an absorber between the coils and the cold bore which reduces the available aperture. In conclusion from 70 mm the aperture for the beam reduces to as low as 39 mm for Q1 to 48 mm for Q2-Q3. Moreover the quadrupoles can have alignments errors up to 2 mm due to the ground motion which reduces again the available aperture.

The aperture of a quadrupole is not a free parameter. In fact it is limited by the gradient that makes the peak field in the coil proportional to the aperture. In superconducting magnets the peak field in the coil is limited and depends on the material used, the magnet field, current and temperature in the coil. For the LHC NbTi magnets the maximum peak field in the coil is about 9 T (see Fig. 3.3.8).



**Figure 3.3.8 Critical surface for NbTi superconductor.**

The LHC triplets, with a gradient of 215 T/m, reach already 7 T at the inner coil diameter that implies a larger peak field at coil.

The tight apertures margins in collision implies that, at injection energy when the beam has a larger emittance due the adiabatic damping (see Eq. 3.2.28), the beams cannot fit inside the aperture in the triplets. Therefore the same  $\beta^*$  cannot be kept at small values at injection and it is much larger (i.e.  $\beta^* = 10$  m). A matching section (see Sec. 3.3.5) which consist of additional quadrupoles is needed downstream to manipulate  $\beta^*$  during the operation.

TAS	Charged particle absorber
BPMSW	Warm Directional Stripline for Q1
MQXA	Q1
MCBX	Cold horizontal/vertical orbit corrector
BPMS	Cryogenic Directional Stripline Coupler for Q2
MQXB	First Q2 module
MCBX	Cold horizontal/vertical orbit corrector
MQXB	Second Q2 module
TASB	Charged particle absorber
MQSX	Skew quadrupole corrector
MQXA	Q3
MCX3	Decapole corrector
MC SOX	Nested skew sextupole, octupole, skew octupole corrector
DFBXA	Triplet Feedbox
BPMSY	Warm Directional Stripline Coupler for DFBXA

**Table 3.1 Elements in the triplet assembly.**

The beta function gives also a measure of the sensitivities of the beam dynamics to mechanical vibrations and field imperfections. For this reason a set of corrector magnets (MC) and beam position monitors (BPM) are placed between the main quadrupoles. Table 3.1 show the full structure.

All these elements (excluding some multipolar correctors for a reason we will see in Sec. 5.8) must be present in all upgrade layouts.

After the matching section the beam enters the arcs. In the arcs the two beams flow in separated magnetic channels (2-in-1 design see Fig. 3.3.9). As Beam 1 and Beam 2 have the same sign for the charge and opposite directions, they need opposite bending fields to have their trajectory curved in the same direction. The separation between the channel is 194 mm for almost all the magnets (including the ones of the matching section). Thus the two beams need to be split and recombined after the triplet. This is achieved by using the separation/recombination dipoles.

### 3.3.4 Separation/recombination section

The separation/recombination dipole section is composed of two dipoles D1 and D2 with the same polarity which bend the particles of the two beam (and the charged debris) in opposite directions (see Fig. 3.3.10 and Fig. 3.3.11).

The neutral debris will instead follow straight and an absorber called TAN (Target absorber neutral) is needed to be put between D1 and D2. D1 is composed of a set of 6 warm common bore magnet modules. They are

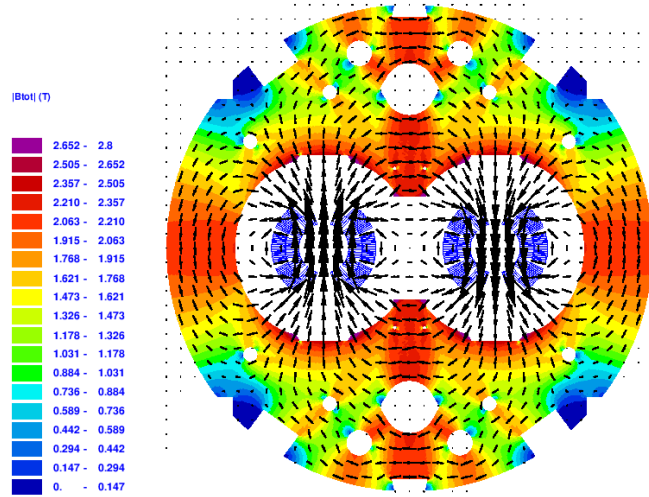


Figure 3.3.9 2-in-1 LHC dipole design.

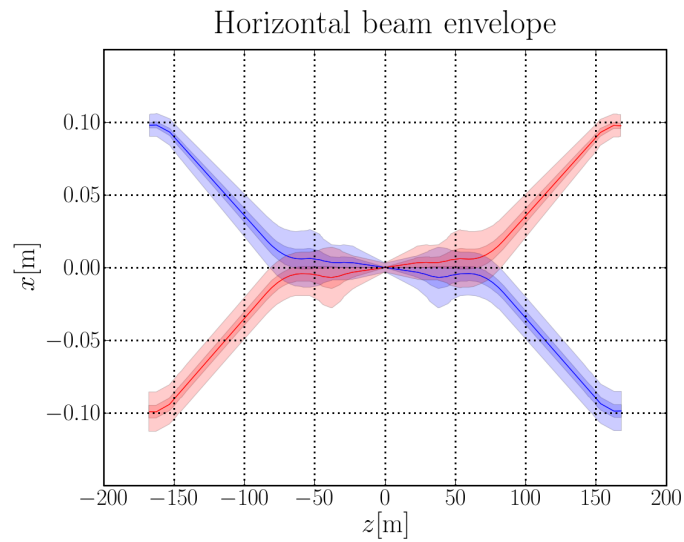
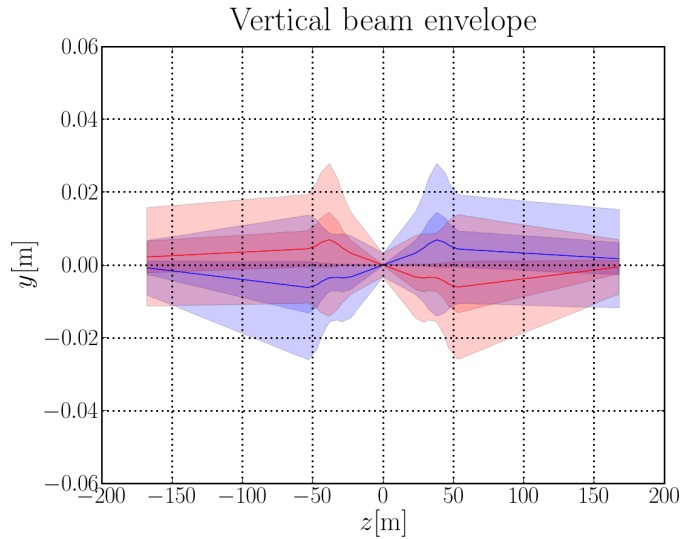


Figure 3.3.10 Beam envelope at  $5\sigma$  and  $10\sigma$  plus tolerances for IR5 in the  $x-s$  plane.



**Figure 3.3.11** Beam envelope at  $5\sigma$  and  $10\sigma$  plus tolerances for IR1 in the  $y-s$  plane.

warm because they have to sustain a high rate of radiation and heat from the debris. D2 is a cold 2-in-1 single dipole. It is shorter than D1 because D2 has a larger peak field.

The aperture required for 2-in-1 magnets can be roughly estimated with the same arguments used for triplets as shown in Fig. 3.3.5. D1 and D2 generate some dispersion that is compensated by the dispersion suppressor. D1 and D2 do not generate the crossing angle  $\theta_c$ , for this purpose the orbit corrector in the triplet and in the matching section are used.

In the LHC the plane of the crossing angle is vertical in IR1 and horizontal in IR5. The reason is in the cancellation of the "pacman" bunches effect, that is the difference of tune between LHC bunches at edge and the core of the bunch train (see [BCL<sup>+</sup>04]).

The crossing scheme generates horizontal and vertical dispersion but it is not foreseen to be compensated. This will add to the spurious dispersion coming from the imperfections in the arcs.

### 3.3.5 Matching section

The matching section is composed by 4 cold 2-in-1 coil quadrupoles (Q4-Q7). The quadrupoles are individually powered in order to allow flexibility in the optics configurations. Q4 and Q5 are cooled to 4.5 K because the heat load is estimated to be larger than in the rest of the matching section, this reduces

the maximum gradient allowed in the quadrupoles. The matching section from Q4 to Q6 is well suited for an upgrade because the region is not as complex and crowded as the dispersion suppressor section.

Figures 3.3.12 and 3.3.13 show the arrangement of the matching section quadrupoles.

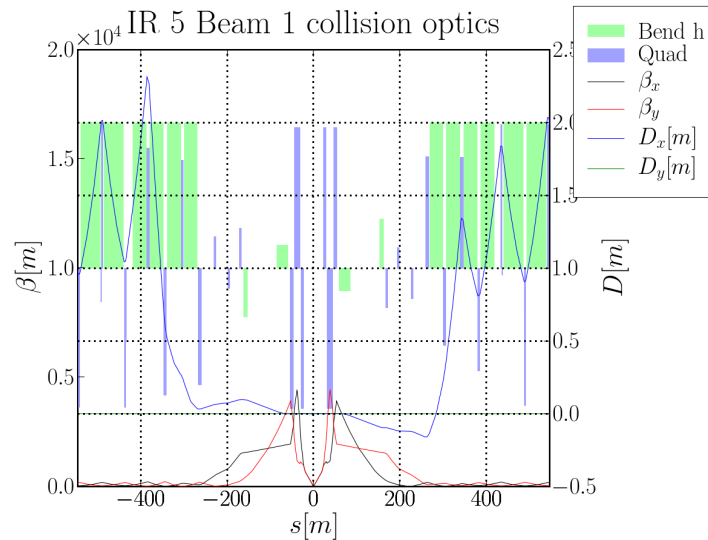


**Figure 3.3.12** LHC IR 5 Beam 1 optics functions. The boxes represent the position, length and polarity of the quadrupoles (blue) and dipoles (green).

### 3.3.6 Dispersion suppressor

The arcs generate dispersion (about 2 m) because of the dipole field. The dispersion must be suppressed to gain aperture in the triplet and to gain luminosity in the IP. The dispersion suppressor uses a compact version of the missing dipole scheme and uses individually powered quadrupoles to compensate the not perfect match of the parameters. In the last two cells of the dispersion suppressor (Q11-Q13), the quadrupoles are powered in series with the arc quadrupole. Individually powered trim quadrupoles (a larger one for Q11) are used to gain optics flexibility.

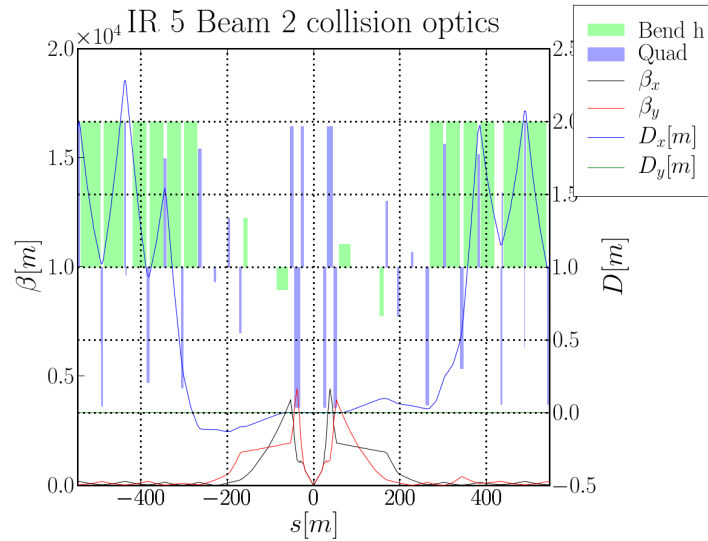


Figure 3.3.13 LHC IR 5 Beam 2 optics functions. The boxes represent the position, length and polarity of the quadrupoles (blue) and dipoles (green).

## 3.4 Limitations of the nominal interaction region layout

Chapter 2 explained how a reduction of the beam size at the IP can increase the luminosity. This section shows what limitations arise when one tries to reduce the beam size using the existing layout.

### 3.4.1 Aperture

The layout of the LHC interaction region is designed to reach  $\beta^* = 55$  cm. If one tries to reduce  $\beta^*$  to 25 cm (for  $\sigma = 11.2 \mu\text{m}$ ), the required apertures in the quadrupoles increases by a factor  $\sqrt{55/25} = 1.48$  (see Eq. (3.3.4)). As the divergence at the IP ( $\gamma^* = 1/\beta^*$ ) increases by reducing  $\beta^*$ ,  $\sigma$  increases proportionally to  $1/\sqrt{\beta^*}$  after the IP.

One may think of reducing the emittance for reducing the beam size, but as shown in Eq. (2.3.2), the beam beam tune shift would increase accordingly, limiting the bunch intensity.

The aperture of the magnet can be increased by changing the magnet technology (e.g. using Nb3Sn which allows a larger peak field) or decreasing the gradient see Sec. 5.8). The last option implies longer quadrupoles as demonstrated in Sec. 5.3.

$D_{x\text{total}}$	Total dispersion,
$f_{\text{spuriousdisp}} = 0.3$	fraction of the spurious dispersion,
$D_{\text{maxarc}} = 2 \text{ m}$	max dispersion in the arc,
$\beta_{\text{maxarc}} = 180 \text{ m}$	max beta function in the arc,
$f_{\text{betabeat}} = 0.2$	beta-beating allowed in the LHC
$\delta_{\text{max}}$	energy spread in the beam
$x_{\text{tolerances}} = 3 \text{ mm}$	closed orbit tolerances

**Table 3.2** Quantities for aperture estimation and values for the LHC.

Another limitation that related to the aperture is the impact of the long range beam beam interaction. If the beam intensity is increased or operations require a small tune spread, the crossing angle could be increased to reduce the effect of the long range beam beam interactions, but the aperture of the quadrupoles will not be sufficient. A possibility to solve the problem is to increase  $\beta^*$  with a loss in luminosity (including the loss due the geometric reduction factor).

In reality the beam occupies a larger region than the first estimation in Sec. 3.3.3 because of machine imperfections, dispersion, orbit misalignments. A formula for a more realistic estimation of the beam size is:

$$D_{x\text{total}}(s) = |D_x(s)| + f_{\text{spuriousdisp}} D_{\text{maxarc}} \sqrt{\frac{\beta_x(s)}{\beta_{\text{maxarc}}}} \quad (3.4.1)$$

$$D_{y\text{total}}(s) = |D_y(s)| + f_{\text{spuriousdisp}} D_{\text{maxarc}} \sqrt{\frac{\beta_y(s)}{\beta_{\text{maxarc}}}} \quad (3.4.2)$$

$$x_{\text{size}}(s) = f_{\text{betabeat}} (n_\sigma * \sqrt{\beta_x(s)} \varepsilon + \delta_{\text{max}} D_{x\text{total}}(s)) + x_{\text{tolerances}} \quad (3.4.3)$$

$$y_{\text{size}} = f_{\text{betabeat}} (n_\sigma * \sqrt{\beta_y(s)} \varepsilon + \delta_{\text{max}} D_{y\text{total}}(s)) + x_{\text{tolerances}}, \quad (3.4.4)$$

where the meaning and the values of quantities appearing are explained in Tab. 3.2

This formula is still not sufficient for a realistic estimation of the aperture margin which requires a 2D aperture model ([BCL<sup>+</sup>04] and [JO97]) which takes into account the geometry of the beam screen and the collimation system.

### 3.4.2 Field quality and long term stability

If we solve the problem of the aperture in the triplet with larger magnets (using Nb3Sn for instance) the peak beta function will still increase by a factor  $1/\sqrt{\beta^*}$ . As discussed in Sec. 3.2.3, the non-linear terms have an effect

which is proportional to some power of the beta function at the location of the perturbation. A larger beta requires a better field quality for the magnets.

Field quality can be improved by increasing the aperture of the quadrupoles ([BKT07]) at the cost of reducing the available gradient.

Field quality can be corrected locally by multipole corrector magnets, but there are fundamental limitations. Firstly it is not possible to put correctors for each multipole because the longitudinal space requirements will be excessive. Usually only the multipole errors which excite the resonances close to the machine tune are corrected (see [BFMG04]). Secondly the effects of the multipoles are weighted with the beta function (the phase advance in the triplet is irrelevant) and a single multipole corrector cannot cancel the contribution exactly. Thirdly, for common bore quadrupoles, both beams must be corrected at the same location, but the correction cannot be optimal for both of them because they have different beta functions there.

### 3.4.3 Beam beam interactions and geometric reduction factor

A reduction of  $\beta^*$  at the IP implies a larger divergence of the beam which reduces the beam beam separation in the region where the beams are in a common beam pipe. In this case the impact of the non linear field would become unacceptable unless the crossing angle is increased. Using Eq. 3.3.5,

$$\theta_c \simeq 450 \text{ mrad} \quad (3.4.5)$$

for  $\beta^* = 25 \text{ cm}$  if the separation is  $9.8\sigma = d_{\text{sep}}\sigma$  at the beam beam encounters.

The increase of the crossing angle has the double effect of reducing the luminosity and increasing the aperture requirements in the triplet. It is worth noting that the beam envelopes overlap at  $d_{\text{sep}}/2(\sigma_{\text{Beam1}} + \sigma_{\text{Beam2}})$  in the triplet if there is no orbit corrector and results in larger or smaller beam beam effect depending whether  $\sigma_1 < \sigma_2$  or not (see 3.4.14).

The nominal LHC has no means (i.e wire or e-lens compensation) for compensating the beam beam interaction which allows a smaller crossing angle or a larger currents to increase the geometric reduction factor for the luminosity. Alternatively crab cavities can rotate the beam in order to force head on collisions (no geometric reduction factor) allowing a larger crossing angle which would allow more current but would require additional aperture in the quadrupoles.

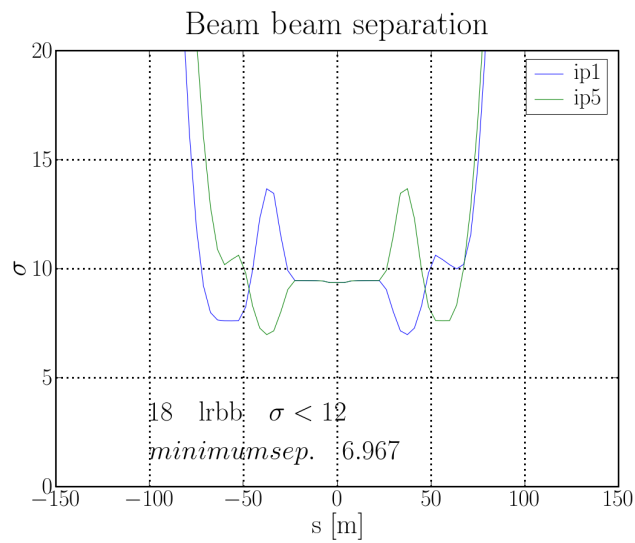


**Figure 3.4.14** Beam beam separation for the nominal LHC. The lines show the separation of the centroids of the beams in multiples of  $\sigma$ . Every 3.75 m there are long range beam beam interactions (lrbb) that are negligible when the separation of the beam is larger than  $12\sigma$ . The separation is not constant and the location where the interactions occurs at small distance are dominant for the beam dynamics.

### 3.4.4 Heat deposition

With an upgrade of the luminosity, the rate of debris generated by beam collisions at IP increases accordingly. The LHC absorbers (TAN and TAS) are designed to reduce the heat load in the superconducting magnet for the nominal luminosity. In case of a luminosity upgrade either the absorber must be redesigned, or the superconducting magnets must be able to sustain a higher heat load or the aperture of magnet must be increased in order not to intercept the debris.

### 3.4.5 Radiation damage

The debris generated at the IP are not only responsible for the heat load, but also for the radiation damage. The LHC triplets lifetime is estimated to be  $700 \text{ fb}^{-1}$  of integrated luminosity which translates into 7 years of operation. The radiation damage must be carefully addressed in order to keep the lifetime of the magnets reasonably high.

### 3.4.6 Chromatic aberrations

As for the long term stability, an increase of the beta function increases the chromatic aberrations. They are responsible for tune dependence on the energy which can enhance the excitation of the resonances and the instabilities.

The linear part must be corrected by the lattice sextupoles. The non linear part is difficult to correct and can drive instabilities and as well decrease the efficiency of the collimation.

### 3.4.7 Matchability

In order to create a small  $\beta^*$ , the beta function at the triplet must be large, but the arcs require a smaller beta. The matching section and dispersion suppressor must therefore be able to transform a small beam with small divergence in the arc into beam with a large divergence in Q4 in order to assure a large beta in the triplet.

If too large beta values are required, the LSS magnets may be limited in strength and aperture. The LSS must also be able to change the optics configuration smoothly between small  $\beta^*$  optics for collision and large  $\beta^*$  optics for injection and ramping at a constant phase advance. Although the number of parameters (individually powered quadrupoles) is larger than the number of constraints, the magnets are often at the limit of their strengths. In addition not all parameters are truly independent or efficient. For instance

---

for controlling the  $\beta_y$  only the quadrupole for which  $\beta_y \gg \beta_x$  are efficient or quadrupoles where  $D_x$  is large are better for changing the dispersion. The quadrupoles must be placed at different phases such that they can control independently several parts of the optics.

### 3.5 Conclusion

In this chapter I showed the basic tools for studying the transverse beam dynamics. The transverse beam dynamics is an essential tool for studying the interaction region layout. An analysis of the limitations of IR arising when one tries to reduce the beam size at the IP introduced the main topic for the design of an interaction region upgrade.

The following chapters develop two different upgrade strategies trying to address and surpass the limitations discussed before. Chapter 4 studies a dipole first layout, an option which inverts the position of the triplets with the separation recombination dipoles. Chapter 5 studies several low gradient quadrupole first layouts in which large aperture and longer quadrupoles are used to overcome the aperture limitation of the present layout.



# Chapter 4

## Dipole first layout

### 4.1 Introduction

In this chapter I discuss the dipole first layout. The advantages and drawbacks are analyzed by studying a realistic layout.

### 4.2 Motivations

As discussed in Ch. 3, some of the limitations of the LHC interaction region are:

- long range beam beam interactions (see Sec. 3.4.3 )
- heat deposition and radiation damage (see Sec. 3.4.4 and 3.4.5)
- correction of field imperfections (see Sec. 3.4.2 and 3.2.3)

Dipole first options try to overcome these limitations by exchanging the position of the triplet and the separation/recombination magnets with respect to the nominal layout.

Dipole first layouts have been proposed first in [BCG<sup>+</sup>02]. Further studies can be found in [dM05], [SSM05], [Bru05], [dMBR06], [SJM<sup>+</sup>06], and [SJRT07].

In the following I develop a dipole first layout in order to check its feasibility in terms of linear optics, field quality specifications, aberrations and long term stability.

### 4.3 Dipole first layout

The new layout has been designed to maintain all the LHC parameters except  $\beta^*$  that is set to 25 cm. All the elements but the triplets and the separation-recombination dipoles are kept the same in order to keep the cost of the upgrade as low as possible. It turned out that Q5, which is not a wide aperture magnet, needs to be replaced due to larger mechanical aperture requirements.

The new magnets require a new technology, such as Nb3Sn superconductor material, which offers a higher peak field in the coils than the one for the nominal layout (15 T as compared to 7 T for NbTi magnets). The requirements for the aperture follow the guidelines explained in Sec. 3.4.1, that is  $10\sigma$  separation of the two beams in order to keep the beam beam interaction small, and  $10\sigma$  from the beam pipe to avoid the beam losses.

The radiation heat load and radiation damage issues have not been taken into account yet, although they are quite important for a realistic design.

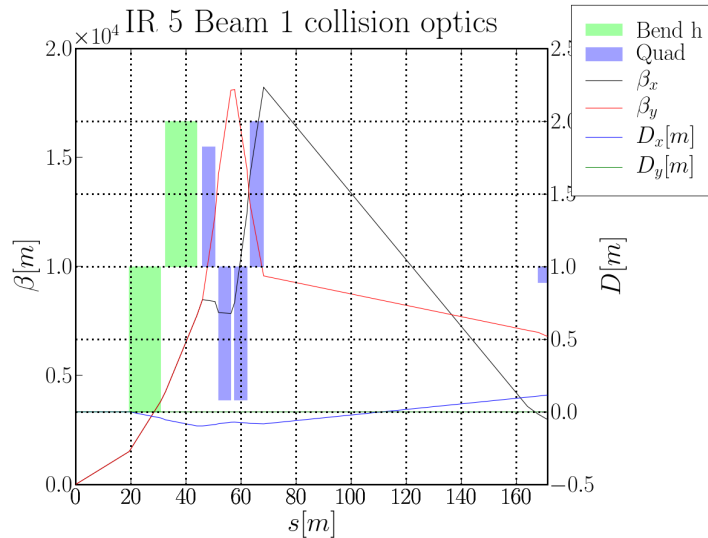


**Figure 4.3.1** Collision optics of a dipole first layout from the IP to Q4. The boxes represent the position, length and polarity of the quadrupoles (blue) and dipoles (green).

Figure 4.3.1 shows the upgraded part of the interaction region, where it is possible to see that the dipoles and the triplets have exchanged positions with respect to the nominal layout (see Fig. 3.3.6). Table 4.1 shows the main specification of the magnets: starting position, length, field and inner diameter.

Mag.	Pos.	Length	Field	Inner D.
D1	19.45m	11.4m	15.0T	130mm
D2	32.653m	11.4m	15.0T	80mm
Q1	46.05m	4.5m	231.0T/m	80mm
Q2A	51.87m	4.5m	-256.6T/m	80mm
Q2B	57.69m	4.5m	-256.6T/m	80mm
Q3	63.25m	5.0m	280.0T/m	80mm

**Table 4.1** Layout specifications for a dipole first upgrade option.

Dipoles D1 and D2, as in the nominal layout, recombine and separate the beam to the nominal separation of 194 mm. In order to reduce the distance from the triplets to the IP, the dipole should provide the highest possible field and enough aperture to reserve the space for the splitting. It has been assumed that the Nb3Sn technology will provide a field of 15 T and an aperture of 100 mm. D2 can be assumed as a two-in-one magnet (see Fig. 3.3.9), because the beams are already separated.

The TAS is a placeholder for an absorber for the radiation coming from the IR. In this layout it should absorb the neutral debris and part of the charged debris as well. The length is taken from the LHC baseline design, that is 1.8 m. The radiation produced by charged particles should be absorbed by D1 whose field acts as a spectrometer deviating the debris along its sides which can be equipped with absorber. A preliminary design is studied in [GAG<sup>+</sup>05] and [Mok05].

The triplet quadrupoles have a two-in-one design. A first design has been proposed in [ZK06].

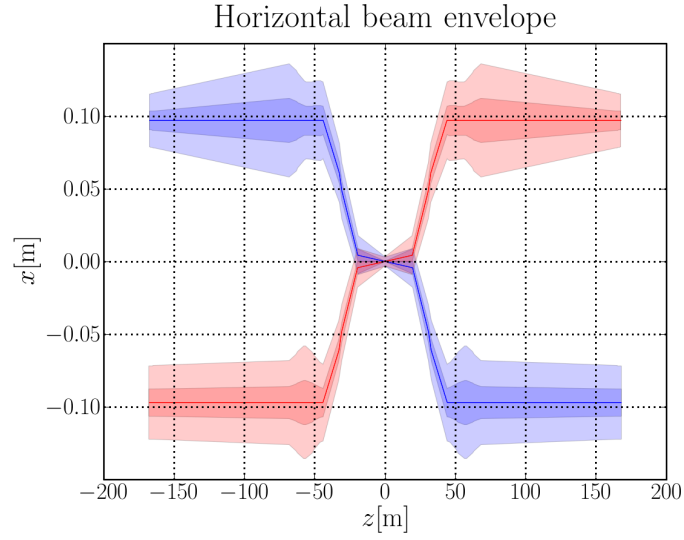
Figures 4.3.2 and 4.3.3 show the beam envelopes for the upgraded layout. As in the nominal layout IR 5 has an horizontal crossing scheme, while IR 1 a vertical one.

All the detailed studies are collected in [dMT]. Only a selection of them will be showed in the following.

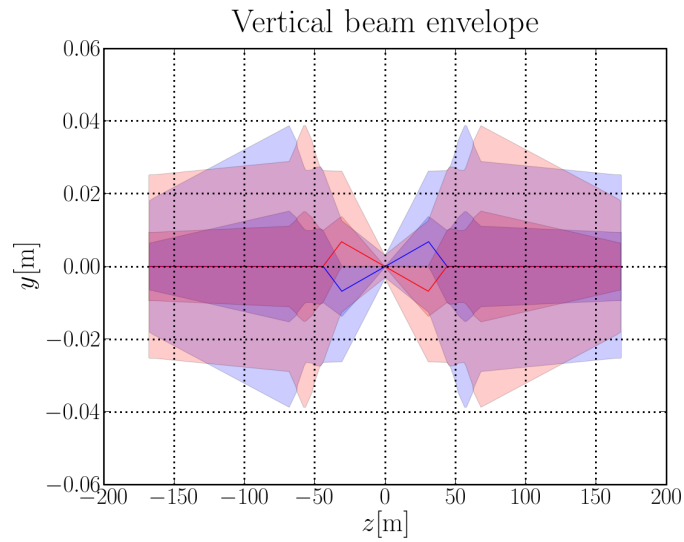
## 4.4 Collision optics

Figure 4.4.4 shows the collision optics for Beam 1. There are several differences with respect to the baseline optics (see 3.3.12 and 3.3.13 ) due the new layout.

The increase of the maximum  $\beta$  function, 18 km compared to the 4 km of the baseline LHC, is due to the decrease of  $\beta^*$  and the increase of the distance from the IP to the quadrupoles (about 46 m instead of 23 m).



**Figure 4.3.2** Beam envelope at  $5\sigma$  and  $10\sigma$  plus tolerances for IR 5 in the  $x-s$  plane. The red and blue lines show the crossing angle in the horizontal plane.



**Figure 4.3.3** Beam envelope at  $5\sigma$  and  $10\sigma$  plus tolerances for IR 1 in the  $y-s$  plane. The red and blue lines show the crossing angle in the vertical plane.

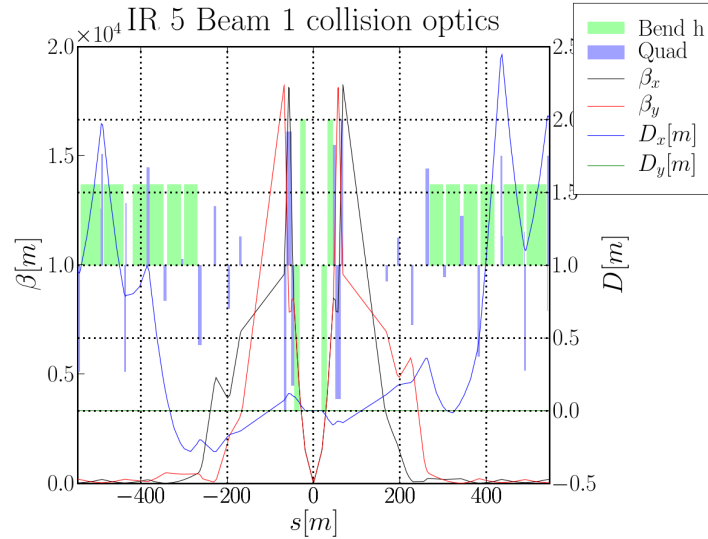


**Figure 4.4.4 Collision optics for Beam 1 in IR 5 for the dipole first layout.**

In the matching region (Q4-Q7) the dispersion (see Sec. 3.2.4) is not zero. This is due to the fact that D1-D2 introduce a dispersion bump that has to be compensated in order to get a zero dispersion at the IP. Dispersion in this region reduces the degrees of freedom of the matching quadrupoles. The dispersion suppressor quadrupoles have to be used for the matching purposes. Moreover the dispersion breaks the symmetry between left and right with respect to the IP and the symmetry between Beam 1 and Beam 2, making the optics solution slightly different for each of these regions.

## 4.5 Crossing scheme

A crossing angle different from zero is needed for the LHC in order to limit the long range beam-beam interactions between the two beams.

The dipole first layouts reduces the number of LRBB to 5 from 15 of the nominal LHC. See Fig. 4.5.5 compared with Fig. 3.4.14.

The value of the angle depends on the separation needed to reduce the long range beam beam interaction (see Sec. 3.4.3, 3.3.1, and 2.3.4). For this layout it has been assumed the same separation in  $\sigma$  that is present in the nominal layout. In these conditions, the reduced number of long range beam beam interaction allows a large bunch intensity and therefore a large luminosity with respect to the nominal.

Table 4.2 shows the values of the crossing angles needed for the base-

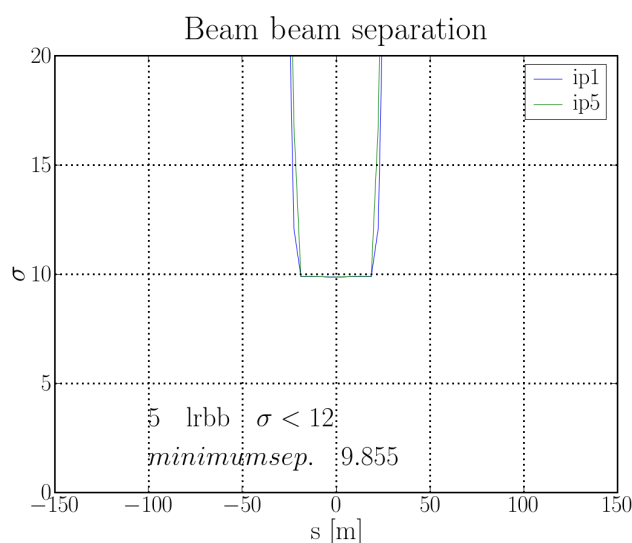


**Figure 4.5.5** Beam beam separation for the dipole first layout.

Data	Unit	LHC	Upg.
Energy	[GeV]	7000	7000
Relativistic gamma		7461	7461
Normalized emittance	[ $\mu\text{m rad}$ ]	3.750	3.750
Emittance ( $\varepsilon$ )	[nm rad]	0.503	0.503
RMS beam size at IP	[ $\mu\text{m}$ ]	16.63	11.21
Half crossing angle ( $\phi$ )	[ $\mu\text{rad}$ ]	142.5	211.4
Half separation ( $d$ )	[ $\sigma$ ]	4.714	4.714

**Table 4.2** Data used for estimating the required crossing angle for the nominal LHC and dipole first layout.

line LHC and dipole first layout LHC in order to fulfill the required beam separation.

The crossing scheme is managed by D1 and D2 and by orbit correctors as in the nominal layout. This is a great advantage because reduces the aperture needs of the triplet magnets and does not introduce spurious vertical and horizontal dispersion. In the LHC the vertical dispersion cannot be corrected and the spurious dispersion propagates in the rest of the machine.

Figures 4.5.6 and 4.5.6 show the crossing schemes for the horizontal and vertical plane. The former can be achieved with a slightly different bending angle for D1 and D2 and the latter by tilting D1 and D2 resulting in a vertical deflection. The dispersion kicks compensate exactly because there is

no quadrupole in between.

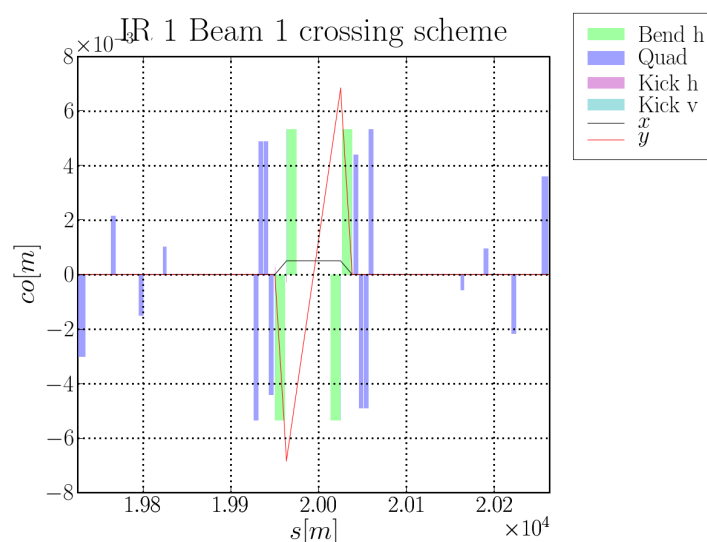


**Figure 4.5.6** Crossing scheme for IR 1 Beam 1 before collision. The lines show the horizontal and vertical displacement of the closed orbit of Beam 1. In the vertical plane the Beam 1 cross the IP with a crossing angle, while in the horizontal plane the beam is displaced to avoid collision with the other beam. During collision the horizontal displacement is removed and the beam collides with a vertical crossing angle.

A separation at the IP is also needed during the injection and the acceleration of the particles. It can be achieved either using the orbit corrector magnets or dividing D1 and D2 in two parts and powering them differently.

Figures 4.5.7 and 4.5.7 show the dispersion function when the crossing angle scheme is on and demonstrate that there is no mismatch outside the interaction region.

## 4.6 Mechanical aperture

Figure 4.6.8 shows the mechanical aperture in term of  $n_1$  (see [JO97]) for this optics. An acceptable value for  $n_1$  in the LHC is  $7\sigma$ . The figure shows that Q5, due to the high  $\beta$  values, needs a bigger aperture. The high values of  $\beta$  are unavoidable due the layout, therefore an upgrade of Q5 to a wide aperture quadrupole (e.g. like an MQY) is necessary.

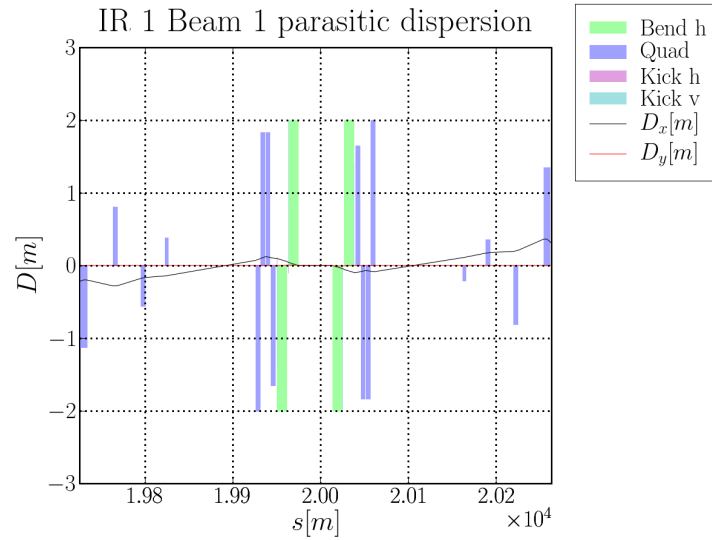


Figure 4.5.7 Parasitic dispersion IR 1 Beam 1. The crossing scheme of dipole first layout does not introduce parasitic dispersion like quadrupole first layouts.

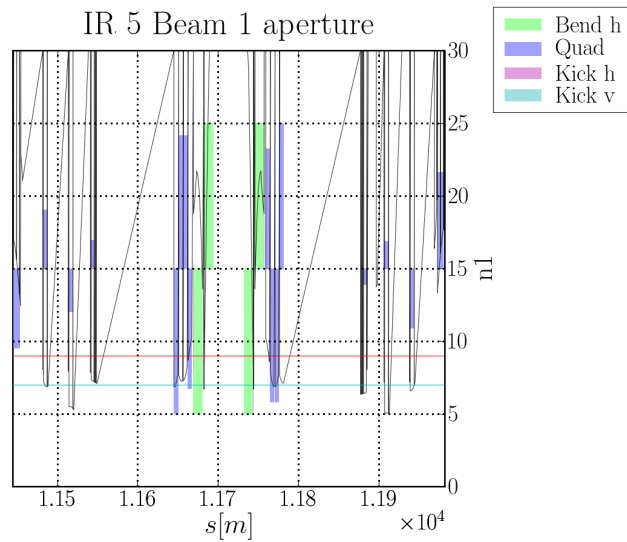


Figure 4.6.8 Aperture margin of IR 5 Beam 1 in terms of  $n_1$ .

## 4.7 Chromaticity

At collision energy, the chromaticity of the LHC (see Sec. 3.2.4 and Sec. 3.4.6 ) is dominated by natural chromaticity of the triplet quadrupoles.

The LHC uses lattice sextupoles for correcting the chromaticity. For each of the 8 arcs in the LHC there are:

- two focusing sextupoles families ( $B_{max} = 1.280\text{T}$  at 17mm),
- two defocusing sextupoles families ( $B_{max} = 1.280\text{T}$  at 17mm),
- one spool piece sextupoles family ( $B_{max} = 0.471\text{T}$  at 17mm).

These elements can be used for correcting the first and second order chromaticity and the off-momentum beta-beat. Their impact on the long term stability is minimized because they are interleaved and at  $\pi$  phase advance.

Figures 4.7.9 and 4.7.10 show the chromaticity and the off momentum beta beat after correction. The first order chromaticity is corrected by the chromatic sextupoles. The second order chromaticity together with the off-momentum beta beat in the triplet and in the half of the machine is corrected by a correct phasing of the IRs as indicated in [Far99].

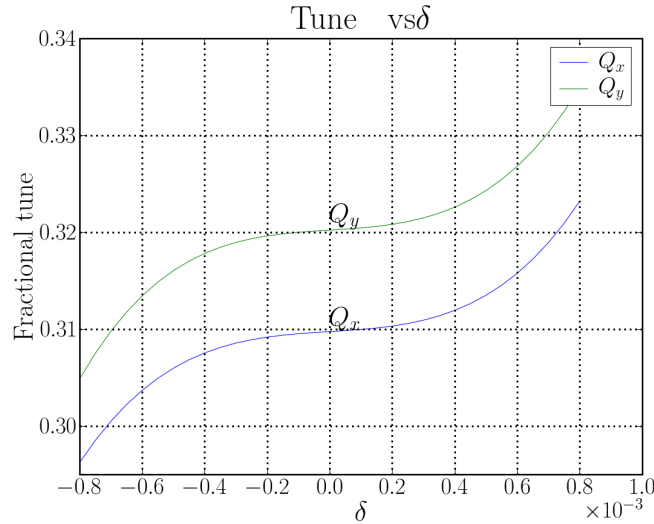


**Figure 4.7.9 Chromatic change of the tune for the dipole first layout. The non linear terms are much stronger with respect to the nominal values.**

Figure 4.7.11 shows the percentage values of the arc sextupoles required for the chromaticity correction. The defocusing values are bigger than the

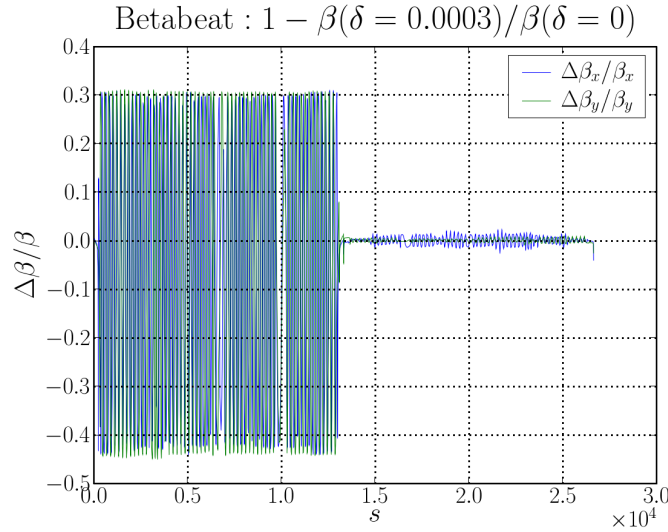


**Figure 4.7.10 Chromatic beta-beating at  $\delta = 3 \cdot 10^{-4}$  for the dipole first layout. The beta-beating is four times larger with respect to the nominal values.**

focusing one because the dispersion is smaller in the location in which they are placed. They use all the available budget.

An attempt to correct the chromaticity (see [dMBR06]) with local sextupoles in the triplet failed due to the large geometric aberrations arising from the strong sextupolar field required for the correction. These components could be compensated by another set of families located where dispersion vanishes and at  $\pi$  phase advance, but there are no suitable places for their installation. The sextupolar field in the triplet can be reduced by a local increase of the dispersion, but the non-linear dispersion emerging from the process spoils the efficiency of the local compensation.

## 4.8 Dynamic aperture

The dynamic aperture (DA) is estimated by tracking an off-momentum ( $\delta = 0.27 \cdot 10^{-3}$ ) particle distribution  $10^5$  turns in 60 realizations of the machine using a statistical model of the multipole field error distribution. The minimum DA among the 60 realizations should give the real dynamic aperture of the machine within a factor of 2 (see the LHC design report [BCL<sup>+</sup>04]). A simulated DA of  $12\sigma$  is therefore satisfactory because the beam-beam interactions and the collimators will limit the aperture to  $6\sigma$  anyway.

At collision the DA is dominated by the field quality of the elements in the

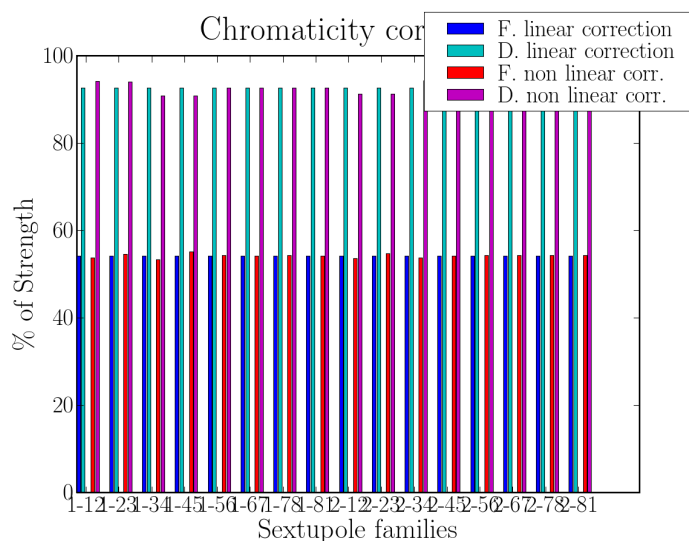


**Figure 4.7.11 Arc sextupole powering for the chromaticity correction. The defocusing families are at the limit of the available budget.**

high  $\beta$  regions: in the quadrupole first designs by the triplets quadrupoles and in the dipole first designs by the triplets and the separation/ recombination dipoles.

The parameter space for a strict specification of the field quality is too large to be explored systematically.

For a first estimation, the DA has been calculated including field errors in the triplet only. Including field errors of the separation-recombination dipoles, while having an important effect on the DA, increases the parameter space enormously and makes it difficult to extend the results to different layouts for which the beta function in these elements is not as large. If not differently stated, the D1/D2 field errors are not included.

The field errors of the rest of the machine should not have a big impact on the DA.

In the studies both high luminosity IR are in collision, no multipole error correction was applied and the beam-beam effect is not included. It has been assumed that each magnet of the triplet follows the same error statistics.

The parameter space has been probed by using the field quality of existing magnets with different scaling laws and using a multipole by multipole scan.

### 4.8.1 DA from measured errors

The present magnet production is used as a reference for the field quality in the tracking studies. The present MQXB is used as prototype for a high gradient quadrupole and the present MQY is used as prototype for a large aperture quadrupole.

Two different scaling laws for the multipole errors are applied. The first is a uniform scaling. The second is expressed by the equation

$$b_n(d_1) = (d_0/d_1)^n b_n(d_0), \quad (4.8.1)$$

where  $b_n(d_1)$  is the relative multipole error of order  $n$  ( $n = 0$  is a dipole) for a magnet of aperture  $d_1$  and the  $b_n(d_0)$  is the relative multipole error for a magnet of aperture  $d_0$ . The reference radius of  $b_n(d_1)$  and  $b_n(d_0)$  is the same. This equation (see [BKT07]) takes into account the geometric scaling of the relative multipoles and the coil precision which does not scale.

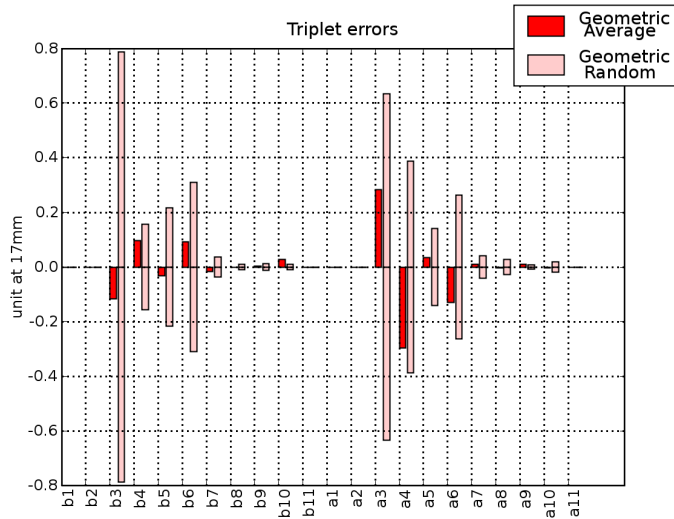


**Figure 4.8.12** Triplet field quality used for the tracking studies. It is equivalent to the present production of the MQXB. The resulting DA is  $3\sigma$ . If the errors are scaled uniformly by 10%, the resulting DA is  $8.3\sigma$ .

Figures 4.8.12, 4.8.13, 4.8.14 show the field quality used for several tracking studies and the resulting DA.

### 4.8.2 Multipole by multipole analysis

An upper bound on the minimum DA can be found by probing one multipole error at the time.

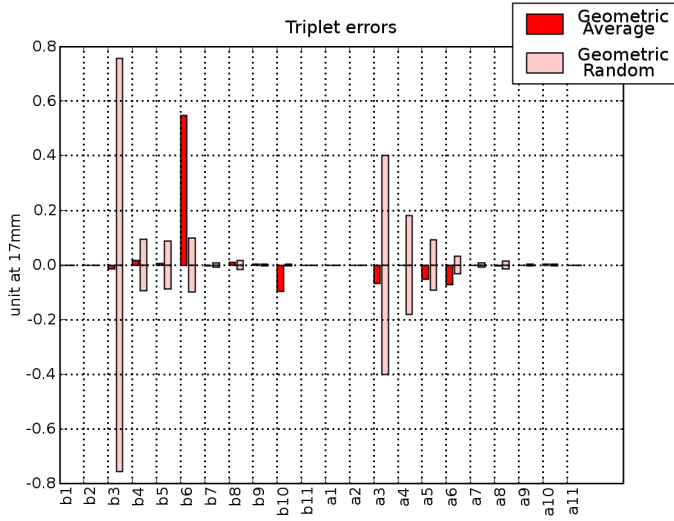


**Figure 4.8.13** Triplet field quality used for the tracking studies. It is equivalent to the present production of the MQY scaled by Eq. 4.8.1. The resulting DA is  $2\sigma$ .

The DA follows a simple scaling law (see [Zie95]) when there is a single multipole error in a machine:

$$\log(d_n) \sim -\frac{1}{n-2}. \quad (4.8.2)$$

where  $d_n$  is the DA in terms of sigma due field errors of order  $n$ .

Figure 4.8.15 and 4.8.16 show the dependence of the DA from the multipole strength where the multipole strength is expressed in term of relative multipole error at two different reference radius.

The curves reproduce the theoretical scaling law. The plot looks more natural when the reference radius is  $12\sigma \simeq 34\text{mm}$ .

The multipoles b6, b8, b10 are dominant and the same effect is observed in the simulation for the nominal LHC.

A tracking study where all the multipoles are set to 1 unit at 34 mm reference radius has been performed and the results shows that the combination of the effects of the single multipoles lead to a DA of  $4.5\sigma$ .

As comparison the DA of the nominal LHC without multipole error correction is  $14\sigma$ .

The results presented here demonstrated that this dipole first layout has an extreme sensitivity to the field quality of the triplet. The specification of the required field errors are beyond the technology reach. Even an efficient

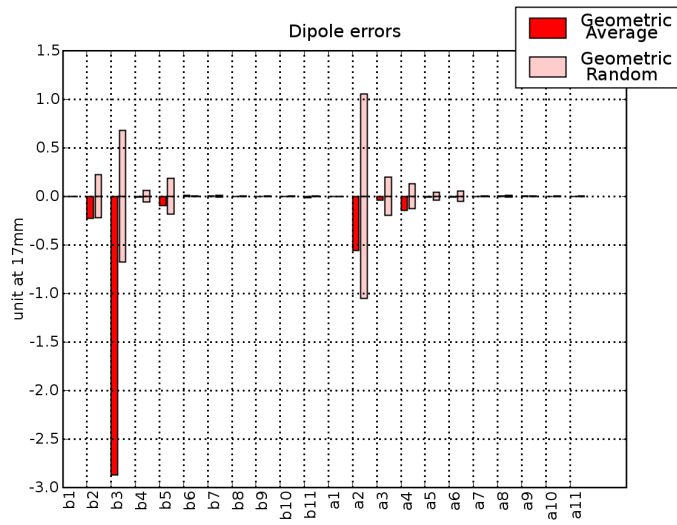


**Figure 4.8.14** Separation recombination dipole field quality used for the tracking studies. It is equivalent to the present production of the cold D2. The triplets has the field quality of the MQXB as showed in Fig. 4.8.12. The resulting DA is  $0.8\sigma$ . If the errors are scaled uniformly by 10%, the resulting DA is  $6\sigma$ .

corrector package allowed by the separated magnetic channel of dipole first layouts will hardly compensate the field error and bring the DA to acceptable levels.

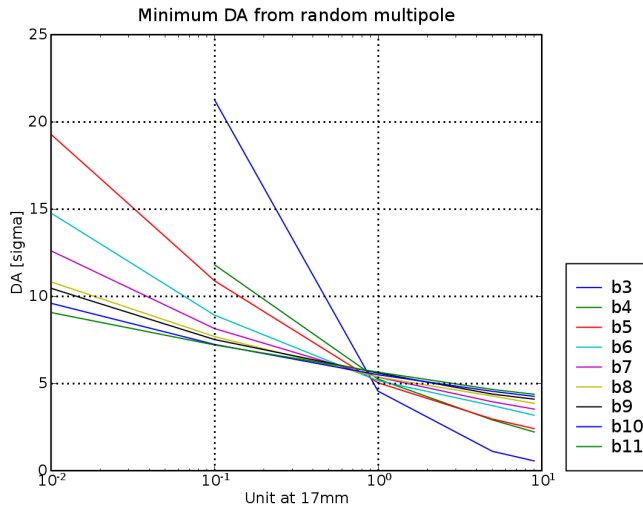


Figure 4.8.15 DA when only a multipole is active as function of the multipole errors. The reference radius is 17mm.

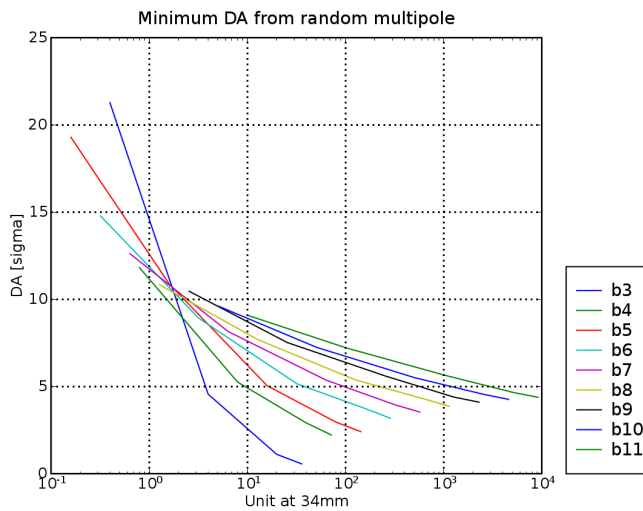


Figure 4.8.16 DA when only a multipole is active as function of the multipole errors. The reference radius is 34mm.

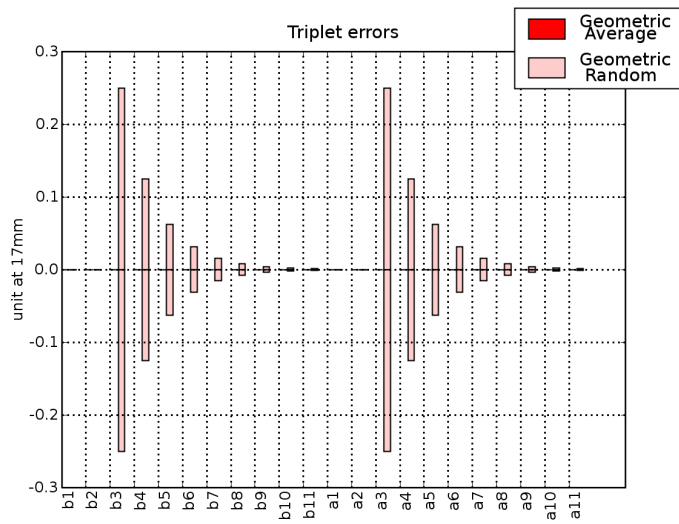


Figure 4.8.17 Triplet field quality used for the tracking studies. It is equivalent to 1 unit at 34mm reference radius. The resulting DA is  $4.5\sigma$ .

## 4.9 Squeeze

The existence of a continuous path of the magnet strengths from collision to injection is not obvious because the strengths of the quadrupoles are close to their limits, the beta functions are high and the dispersion in the matching section reduces the available degrees of freedom.

For this particular layout a solution has been found using a new matching routine in MADX able to cope the complex boundary conditions arising from the broken symmetries and the barely sufficient flexibility of the LHC optics (see [dMSS06] and Appendix A).

Figure 4.9.18 shows the strengths of the quadrupoles during the transition.

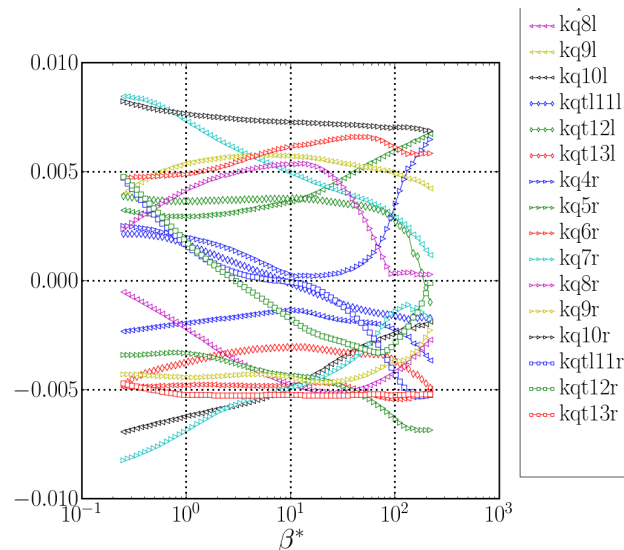


**Figure 4.9.18** Strengths of the IR 5 Beam 1 matching quadrupoles as a function of  $\beta^*$ . The evolution of the quadrupole strengths is smooth but with some inversion of the slope which might be a problem because of hysteresis effects in the multipole errors.

The evolution of the quadrupole strengths is smooth but with some inversion of the slope which might be a problem because of hysteresis effects in the multipole errors.

## 4.10 Conclusion

A dipole first scenario with the relevant optics configuration has been developed. The required aperture is compatible with the element specifications.

Q5 should be replaced with an MQY magnet type. The crossing schemes are completely managed by D1/D2 and there is no dispersion mismatch due the crossing angle.

The linear and second order chromaticity can be corrected by the sextupoles in the arcs. The third order chromaticity poses a limit for the operational margins (i.e. chromaticity measurement). The off-momentum beta-beat is under control in the triplet but not in the arc. It should be possible to compensate it using the available budget of sextupole strength.

The field quality of the present magnet production alone cannot assure the required DA. The better field quality expected from a large aperture does not help.  $b_3$  seems responsible for the lowest DA but scales quickly.  $b_6$ ,  $b_8$ ,  $b_{10}$  scale slowly and might represent a bottle neck. The multipole errors should be smaller than 1 unit at 34mm for upgrade scenarios where the maximum beta function is larger than 18km. An effective corrector package is needed to reach the required DA.

The radiation damage due the debris has not been addressed yet. The layout allows a natural magnetic TAS (racetrack magnets) for the charged debris. It is not clear how to cope with neutral debris.

In conclusion the dipole first layout studied, while assuming an optimistic improvement of the magnet technology, requires extremely tight field quality specification in order to preserve the long term stability. The chromatic aberrations are just on the limit of ability to correct them and high order terms may reduce the performance of the LHC. The layout assumes optimistically that the heat load and radiation damage can be reduced by an optimized protection systems whose feasibility has not demonstrated yet.

For these reasons the dipole first options has been considered too challenging to implement in practice . In order to make a comparison, the following chapter will study quadrupole first options whose main driving criteria is the technical feasibility using the existing technology.

# Chapter 5

## Quadrupole first layouts

### 5.1 Introduction

In this chapter I discuss quadrupole first layout options. I developed and used an analytical tool for a parameter survey of the performance of the quadrupole first layout options and for designing optimized layouts. I studied different realistic layouts that are designed to address different design criteria. The advantages and drawbacks of quadrupole first options are analyzed by studying the performance of the layouts.

### 5.2 Motivation

As discussed in the Ch. 3 some of the limitations of the nominal interaction region are:

- aperture limitations (see Sec. 3.4.1);
- heat deposition and radiation damage (see Sec. 3.4.4 and 3.4.5);
- field quality (see Sec. 3.4.2 and 3.2.3);

Quadrupole first layout options try to overcome these limitations by using longer and weaker magnets requiring magnets compatible with the existing technology.

### 5.3 Optimization of triplet layout

The design of quadrupole first layouts requires a careful optimization of the focusing system assembly.

First results (see [dMB06]) gave an indication that weaker and longer magnets can fulfill the requirements of the upgrade with existing magnet technology.

However, these type of layouts enhance the chromatic effect and integration issues with the matching section, which are already enhanced by the reduction of  $\beta^*$ , because the beta function in the triplet becomes larger as compared to focusing systems which uses short and stronger magnets.

Therefore, it is important to find the final focus layouts which minimize the beta function in the quadrupoles. At this stage of the design, it is also important to identify the theoretical limitations in order to ensure that the found solutions are optimal and also for giving directions to technology R&D.

The analysis that follows is not limited to triplets only, but tries to study multiplets with any number of quadrupoles. From now on I will call final focus system the set of magnets that focus the beam before the collision point. In this sense the LHC triplets are a final focus system.

Several papers and reports have been written on the design and optimization of quadrupole multiplets topic, see [Reg67a], [Reg67b]. Although the results are useful as calculation tools for the analysis of a layout (in particular when the computational resources were limited), they are not suited for the design process of a final focus system for the LHC due to the complexity of the formulas which relate the layout parameters with the performance goals.

An approach, used in particular for linear collider by taking advantage of the symmetries in the layout and using thin lens approximation, (e.g. [BS84], [BS87] and more recently [RS01]) allows to optimize the chromatic and geometric aberrations by using non-linear elements and to achieve very small spot size, but leads to longer and more complex structures compared to the ones involving only linear elements. In circular colliders, this approach has not been yet proved to be satisfactory due to the space limitations which do not allow efficient layouts and to a non-exact cancellation of the aberrations which limits the dynamic aperture (see [dMBR06]).

Other studies used several approximations (e.g. thin lens approximation in [dG97] and [dG98] ) and restricted the analysis to some particular cases (e.g. coarse parameter scan for the SSC in [Peg84] or symmetric triplets for the LHC in [dG97], [dG98] and [KRT07]) in order to decrease the complexity of the equations and reduce the dimensionality of the parameter space. This strategy exposes the studies to the chance of missing the true optimum and does not answer the question of what are the limitations induced by a magnet technology independently on the details of a given layout. In fact, the thin lens approximation is not always accurate and usually requires a refinement using the exact thick lens theory that spoils the generality of the results.

A symmetric triplet is a layout that offers good performance (e.g. in the nominal LHC), but not in all possible scenarios.

We will now see how to write the equations needed to solve for designing an optimized final focus systems.

### 5.3.1 Final focus design

Final focus systems are supposed to invert the sign of the divergence of the beam ( $x'(s)$  and  $y'(s)$ ) which tends to defocus the beam when it is seen coming from the IP.

In terms of Twiss parameter the focusing system must invert the sign of  $\alpha$  in both plane. The exact values for  $\alpha$  at the of the final focus system depends on the peak beta function and the position and aperture of the quadrupoles in the matching section.

The conditions for  $\alpha$  translate in two equations. These equations can be relaxed in inequalities, assuming that the matching section will be able to absorb a range of values. For the LHC this assumption is weak for the reason discussed in Sec. 3.4.7.

#### Initial conditions

The design of a final focus system starts from the definition of the initial condition in the IP. Section 2.3 shows that the transverse beam sizes at the IP of the colliding beams must be equal for maximizing the luminosity. The transverse beam sizes at the IP depends on the vertical and horizontal emittance and vertical and horizontal beta function.

Hadron machines exhibits the same emittance in both planes because there is no strong natural mechanism that affect the emittance in one particular plane, as opposed to lepton machines where the synchrotron radiation damps the motion only in the horizontal plane. It implies that both beams must have the same beta functions.

Section 2.3.4 shows that elliptical beams optimize the luminosity, but it is not easy to generate elliptical beams using quadrupole first layouts in the LHC. The reason is that the region occupied by the beam must be as round as possible to use efficiently the round aperture of the quadrupole. In case of quadrupole first layouts both beam uses the same quadrupole field, but as the charge is the same but the momentum opposite, the two beams will experience opposite force. For instance, if a quadrupole is focusing for Beam 1 in the one plane, it will be defocusing for Beam 2 in the opposite plane. This symmetry implies that if one optimize the aspect ratio of Beam 1 to be round in the triplet and elliptic in the IP, it will automatically distort

Beam 2 that will not be optimized as well. Only round beams at the IP optimize the aperture of the quadrupole. There is then a trade off between the ellipticity that optimize the luminosity and the roundness that optimizes the aperture. For the LHC, the particular shape of the beam screen which has not a circular symmetry allow an optimization of both the aperture and the luminosity as shown in [Far09] using slight elliptic beams.

In conclusion optimized layouts should generate round beams with the same beta function in both planes, therefore in the literature it is common to refer to  $\beta^*$  has a single quantity.

### Minimizing the peak beta function

For finding the layout that minimizes the peak  $\beta$  function with the limitation that the peak field in the coil is fixed, it would be necessary to have magnets whose aperture and gradient be a continuous function of  $s$ . This is not possible for technological reasons, therefore we have to assume that the gradient and the aperture are fixed within a magnet module.

In order to generate round beam, final focus system must provide approximately the same focusing strength in both planes. Only a set of three or more quadrupoles can guarantee equal focusing properties in both planes, therefore we will concentrate on multiplets with a number of quadrupoles larger than 3.

This assumption simplifies the optimization problem, but it would require different magnets with different cross sections. For cost reasons in terms of R&D and spare policies, it would be better to use magnet with the same aperture, the same gradient and the same length. In this way the number of parameters reduces and the effectiveness of the optimization reduces as well. In the rest of the chapter we will see several options with different balances of modularity and optimizations.

Using these assumptions the optimization problem translates in imposing that the peak of the beta functions and the absolute value of the gradient will assume all the same value. In this way all the quadrupoles will exercise the all the available focusing leverage because the edge of the beam will see always the maximum bending field. The number of peak of the beta function depends on the number of quadrupoles in the multiplets. For triplets the peaks are 2 because the beam should see a bending field of opposite polarity in two planes (see Fig. 5.3.2). For quadruplets the number of peaks are 3 and so on.

The requirements for optimization translate in  $n - 2$  equations where  $n$  is the number of quadrupoles.

### 5.3.2 Parameters

In conclusion for a given multiplet optimization we have  $n + 1$  equations and  $n + 1$  parameters. The parameters are  $n$  lengths of the quadrupoles  $l_i$  and the normalized gradient  $k$ . The layout equations depend on the initial condition  $L^*$ ,  $\beta^*$ , which determine the boundary conditions for the Twiss parameters at the beginning of the final focus system. The final conditions for  $\alpha$  at the end of the final focus system represent other two parameters. However their values are extremely difficult to specify because they depend on the ability of the matching section to manipulate the beta function using the strengths of the quadrupole (20 parameters in total) while being compatible with the hardware constraints. No study has been done yet to clearly specify those conditions, because the set of allowed values of the matching section parameter strengths has the form of not connected hyper surfaces of a large number of dimensions.

In order to continue the general treatment we assume that at the boundary of the final focus  $\alpha_x = \alpha_y = 0$ . In other words we will now look for point to parallel final focusing systems, where the point is the IP and the beam trajectories are become parallel after the focus system. These hypothesis allow us to find the minimum beta function that a final focus can achieve in theory. Any focusing boundary conditions for which  $\alpha > 0$  will results in a larger peak function because the quadrupoles must focus more, thus be longer (the peak field is fixed) thus they defocus more in the other plane and they make the peak beta grow.

Another simplifying hypothesis is to leave no empty space between the quadrupoles. While technologically impossible, the hypothesis allow a general treatment of the problem. As additional drift spaces result in an increase of the beta function, gap-less final focus system will always features the smallest possible beta peaks.

Using gap-less parallel to point focusing system the problem depends now only on  $\beta^*$ ,  $L^*$ ,  $k(s)$  and the quadrupoles lengths  $l_i$ .

### 5.3.3 Approximation of the equations

As explained in Sec. 3.2.2, Eq. 3.2.14 or Eq. 3.2.16 can be used to find the dependance of the beta function on the focusing properties of a lattice  $k(s)$ . There are several analytical and numerical methods for solving this equation using a matrix approach (see for instance [CT99]). The challenge is to find parameter dependent solutions.

A full analysis of the problem can be found in [dM07a] and reference therein. The strategy explained and adopted in this paper use a well justi-

fied approximation that simplifies the equations and allows write the problem in dimensionless quantities. The dimensionless problem can be solved numerically and the actual quantities can be scaled back.

In the following part I sketch the main passages.

Let  $w_x = \sqrt{\beta_x}$  and  $w_y = \sqrt{\beta_y}$ , then using Eq. 3.2.16:

$$w_x''(s) + k(s)w_x(s) - \frac{1}{w_x^3(s)} = 0 \quad (5.3.1)$$

$$w_y''(s) - k(s)w_y(s) - \frac{1}{w_y^3(s)} = 0, \quad (5.3.2)$$

where  $k(s)$  is the normalized quadrupole strength and the sign changes depending on the plane.

In a final focus system, the high order term can be neglected because  $1/w^3$  is often a small number compared to the variation of  $w$  over  $s$  and  $k(s)w_x(s)$  in a focus system. Last equations (Eq. 5.3.1 and 5.3.2 ) assume the form of

$$w''(s) \pm k(s)w(s) = 0 \quad (5.3.3)$$

and, if  $k$  is constant, a solution has the form of

$$w(s) = w_0 \cos(s\sqrt{|k|}) + \frac{w'_0}{\sqrt{|k|}} \sin(s\sqrt{|k|}) \quad (5.3.4)$$

or

$$w(s) = w_0 \cosh(s\sqrt{|k|}) + \frac{w'_0}{\sqrt{|k|}} \sinh(s\sqrt{|k|}) \quad (5.3.5)$$

, depending on the sign of  $\pm k(s)$ .

A first application allows to find the maximum of  $\beta$  inside a focusing quadrupole. If the approximation is valid and if this maximum is not trivially on one of the two extremities, the maximum  $\beta$  in a quadrupole can be found solving the system:

$$w_m = w(s_m) = w_0 \cos(s_m\sqrt{|k|}) + \frac{w'_0}{\sqrt{|k|}} \sin(s_m\sqrt{|k|}) \quad (5.3.6)$$

$$0 = w'(s_m) = -w_0\sqrt{|k|} \sin(s_m\sqrt{|k|}) + w'_0 \cos(s_m\sqrt{|k|}). \quad (5.3.7)$$

which is equivalent to

$$\tan(s_m \sqrt{|k|}) = \frac{w'_0}{w_0 \sqrt{|k|}} = -\frac{\alpha_0}{\beta_0 \sqrt{|k|}} \quad (5.3.8)$$

$$\beta_m = w_m^2 = w_0^2 + \left( \frac{w'_0}{\sqrt{|k|}} \right)^2 = \beta_0 - \frac{\alpha_0}{\beta_0 k} \quad (5.3.9)$$

where  $\beta_m = w_m^2$  is the maximum  $\beta$ ,  $s_m$  is the location where the maximum occurs,  $w_0 = \sqrt{\beta_0}$  and  $w'_0 = -\alpha_0/w_0$  are the initial conditions at the beginning of the quadrupole.

### 5.3.4 Normalization

We can now define dimensionless quantities  $\theta, \bar{w}(\theta)$  defined by

$$\theta = s \sqrt{|k|} \quad w(s) = \bar{w}(\theta) \quad \bar{w}'(\theta = 0) = 1 \quad (5.3.10)$$

In this case Eq. 5.3.1 and 5.3.2 become:

$$\bar{w}''(\theta) + \bar{k}(\theta) \bar{w}(\theta) = 0, \quad (5.3.11)$$

where  $\bar{k}(\theta) = \pm 1$  depending whether at  $\theta$  there is a focusing or defocusing quadrupole and the solution are a series of circular and hyperbolic rotations (see for instance Fig. 5.3.1).

As Eq. 5.3.11 is linear and homogeneous, the solution depends only on the ratio of the initial conditions that is

$$\bar{w}_0/\bar{w}'_0 = \sqrt{|k|} w(L^*)/w'(L^*) = L^* \sqrt{|k|} \quad (5.3.12)$$

, because

$$w(L^*) = L^*/\sqrt{\beta^*} \quad w'(L^*) = 1/\sqrt{\beta^*} \quad (5.3.13)$$

### 5.3.5 Scalings

Using this property we can solve the optimization problem using the initial conditions  $\bar{w}'_0 = 1$  and varying  $w_0$  from 0 to  $\infty$  and use

$$L^* \sqrt{|k|} = \bar{w}_0 \quad (5.3.14)$$

$$w(s) = \bar{w}(\theta) \sqrt{\beta^*} \sqrt{|k|} \quad (5.3.15)$$

$$\sqrt{|k|} l_i = \theta_i, \quad (5.3.16)$$

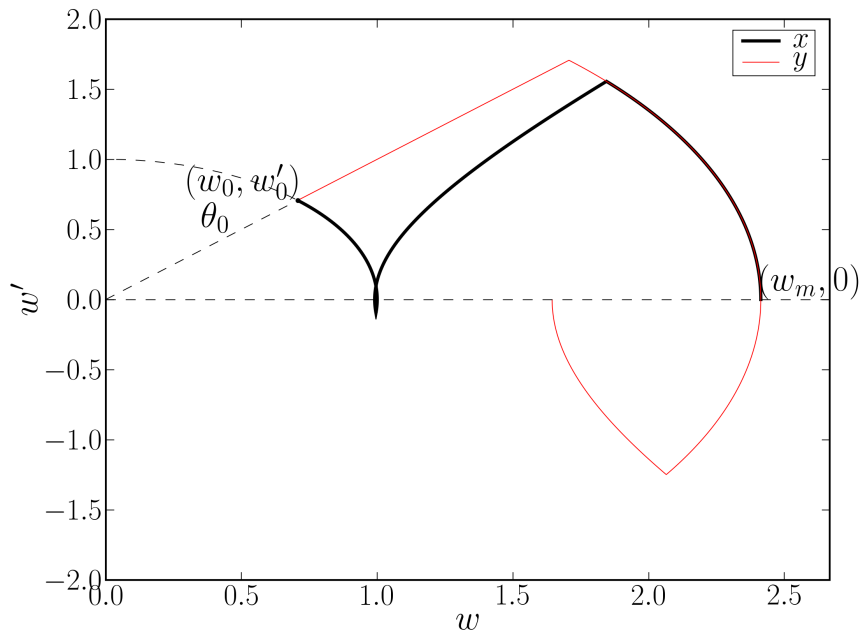


**Figure 5.3.1** Phase space diagram for a point to parallel constant gradient triplet with initial condition  $w_0 = \sin(\theta_0), w'_0 = \cos(\theta_0), \theta_0 = \pi/4$ . The curves show  $w = \sqrt{\beta}$  in the  $(w, w')$  space. The black curve ( $x$ ) is composed by a sequence of a circular, hyperbolic and again circular rotation which represents a sequence of a focusing, defocusing and again focusing quadrupole. The red curve on the contrary ( $y$ ) is composed by a hyperbolic, circular and hyperbolic rotations. The circular rotation for the  $y$  coordinate and the last circular rotation for  $x$  on the right side of the figure overlaps because one has imposed that  $\max(\beta_x) = \max(\beta_y)$ . The point  $(w_m, 0)$  identifies the maximum  $\beta$ .

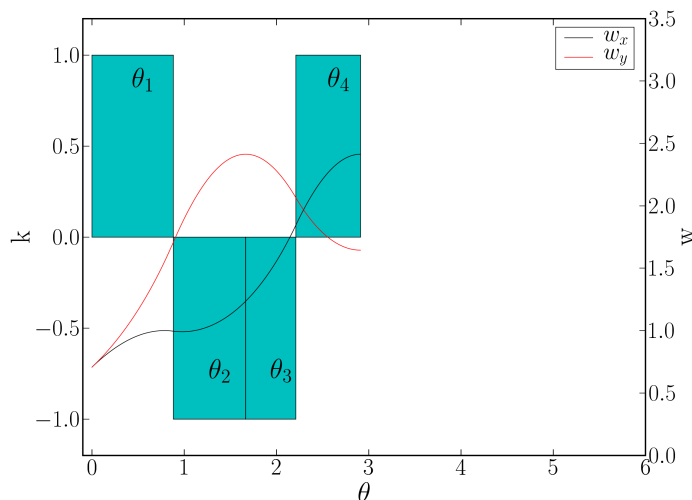


**Figure 5.3.2** Point to parallel constant gradient triplet. The boxes represent the position, length and polarity of the quadrupoles.

to solve Eq. 5.3.1.

The optimization equation can now be written in the case of a triplet as:

$$\bar{w}'_x(\theta_4) = 0 \quad \bar{w}'_y(\theta_4) = 0 \quad \bar{w}_y(\theta_2) = \bar{w}_x(\theta_4) \quad \bar{w}'_x(\theta_2) = 0, \quad (5.3.17)$$

where the first two equations represent the point to parallel focusing and the last two equations represent the minimization of the beta function.

The solution of the system for a given initial condition is shown in Fig. 5.3.2. For a range of initial conditions the solution the solution is shown in Fig. 5.3.3.

The function  $\bar{w}_m(\bar{w}_0)$  can be fitted using:

$$\bar{w}_{\max} \simeq 2 + 1.21e^{-\bar{w}_0} + \bar{w}_0. \quad (5.3.18)$$

This gives the analytical solution of the initial problem - what is the minimum peak beta function that a final focus system show using quadrupoles with a given gradient - by using the scalings:

$$\beta_{\max} = \frac{\bar{w}_{\max}^2}{\beta^*|k|} \quad \bar{w}_0 = L^* \sqrt{|k|} \quad (5.3.19)$$

The method can be used for multiplets with any number of quadrupoles. It is possible to show that quadruplet and multiplets have smaller peak beta

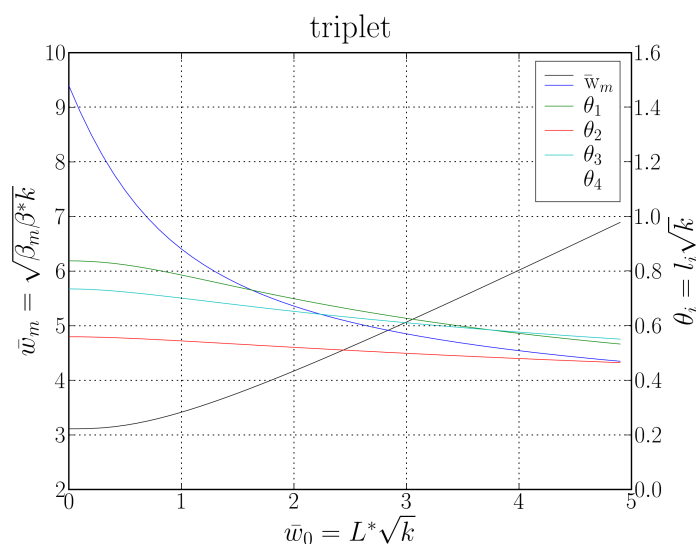


**Figure 5.3.3 Solution for a triplet final focus system.** The figure shows the normalized lengths  $\theta_i = l_i \sqrt{|k|}$  and the maximum  $w = \sqrt{\beta}$  as a function of the initial conditions parameterized according to  $\bar{w}_0 = L^* \sqrt{|k|}$ .

functions with respect to the triplets, but they results in much longer structure. The chromatic aberrations, on the contrary, do not depend on the number of quadrupoles in the multiplets. The triplets therefore represent a favorable solution.

### 5.3.6 Parameter space

Using Eq. (5.3.19 and 5.3.18, it is possible to plot the maximum beam size of the beam in the triplet as a function of the gradient using the simplified model. This function divides the plane in a region where the focusing systems that have a negative focal length (above the black line in Fig. 5.3.4) and the one having positive focal length.

It is possible to draw in the same plot the region of the aperture and gradient compatible with NbTi magnets (red region). A rough estimate impose a the peak field of 8 T at the edge of the beam region diameter  $a$  defined by  $a = 33\sigma + 22$  mm.

Figure 5.3.4 shows that if the gradient decrease the aperture required by the beam increases slower than the aperture compatible with a given peak field. It implies that the smaller is the gradient, the larger will be the aperture margins. The clear advantage of low gradient quadrupole magnets is limited by the fact that the quadrupoles needs to be longer, the beta

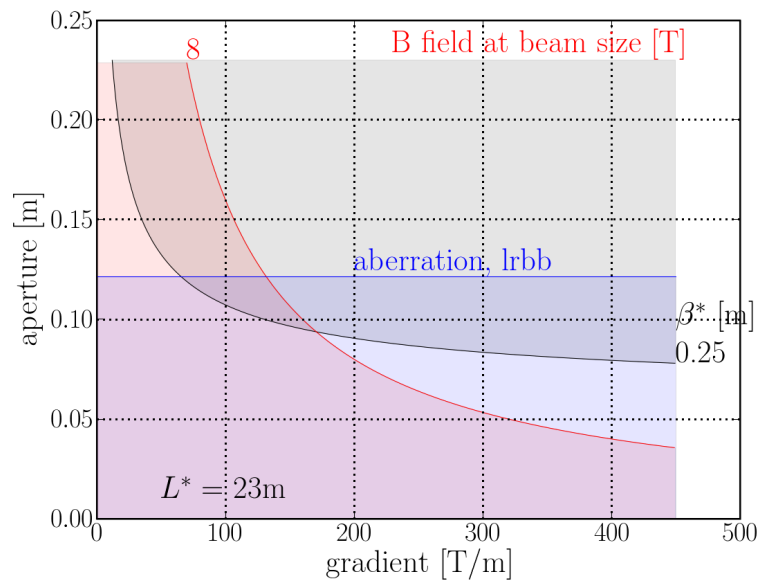


Figure 5.3.4 Triplet parameters space for the LHC upgrade. The intersection of the three shaded regions contains all the possible apertures and gradients compatible with a final focus system using NbTi quadrupoles. The blue region represents the intrinsic focusing limitations of a triplet assembly. The red region represents the limitation of the NbTi technology that cannot hold peak field in the coil larger than 8 T. The gray region represents the limitations of the intrinsic aberrations (natural chromaticity and long range beam beam interactions) of the final focus system.

functions become larger and the chromatic aberrations increase. Another disadvantage is that the number of long range interaction increases as well. For this reason Fig. 5.3.4 show another region (blue) delimited by a line which represent a rough estimation of the above mentioned limits.

The simplified model gives an indication of the parameters of possible focusing systems. However a realistic implementation is necessary to test the hypothesis and identify further limitations.

## 5.4 Four flavors of quadrupole first layouts

Four layouts that span the parameter space and modularity for NbTi technology are proposed and studied extensively in order identify and quantify the merits and challenges.

A study has been performed to identify the possibilities for a replacement of the nominal triplet ( see [dM07a]). Four different layouts have been proposed (see [KRT07] and [BdMO07]) in order to explore the parameter space and identify the benefits and limitations of several design criteria.

Once the gradient is fixed, is necessary to introduce gaps between the quadrupoles in order to make room for coil ends that do not contribute to the field and magnet interconnections. Additional room can be reserved for corrector packages.

The optimal quadrupole lengths are in general different for every unit; one has to trade the aperture margins and the overall lengths with the possibility of using equal sized modules that reduce the cost of the equipment in terms of R&D and spare policy. It is worth noting that the nearest quadrupole to the IP always requires a smaller aperture. Therefore it is possible to use a stronger quadrupole with a smaller aperture and the same peak field with respect to the other units resulting in a gain in the overall length and the beta peak. Also in this case it is possible to trade this optimization with the cost of the equipment and the spare policy. In addition the larger aperture margins of the first unit can be used to install thick shielding tubes that protects the coils from the debris coming from the collisions.

Four different layouts (see Fig. 5.4.5, 5.4.6, 5.4.7, 5.4.8) were designed and studied using different gradients and modularity options.

All data and analysis are collected in [dMT], only a selection is showed in the following parts.

**Compact** This option (see Fig. 5.4.5) uses a triplet layout and the lowest possible gradient compatible with tolerable aberrations. The overall length is minimized (the name comes from there) using an optimized

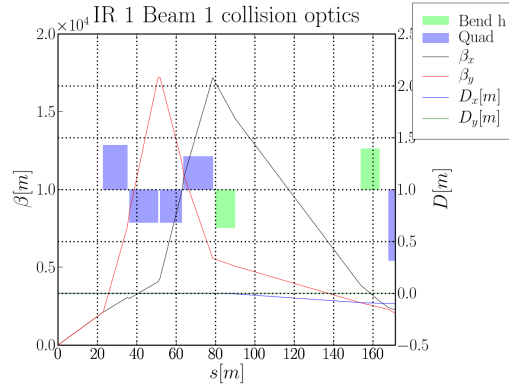


Figure 5.4.5 Upgraded IR layout: “Compact”. The layout is optimized to feature the largest aperture margin and be as compact as possible.

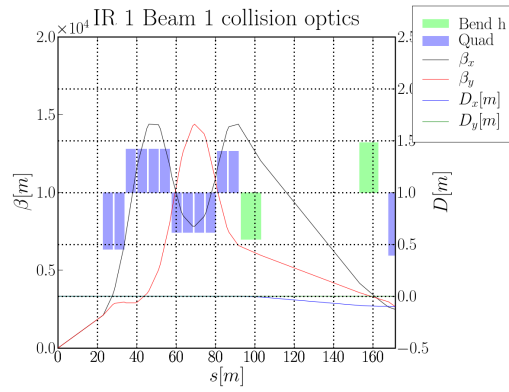


Figure 5.4.6 Upgraded IR layout: “Modular”. The layout is designed to have the quadrupole modules of the same lengths.

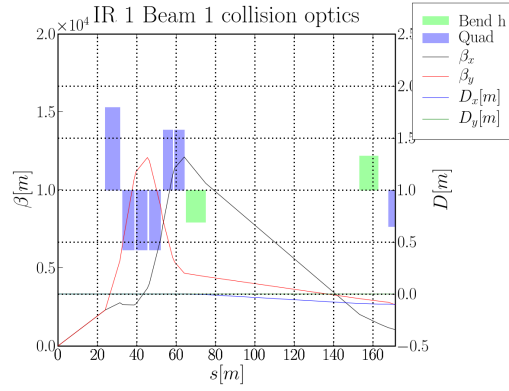


Figure 5.4.7 Upgraded IR layout: “Lowbetamax”. The layout is designed to reduce the peak beta function.

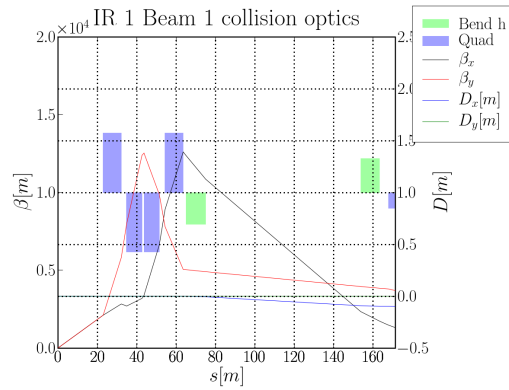


Figure 5.4.8 Upgraded IR layout: “Symmetric”. The layout is designed to have the smallest peak beta function compatible with only two module lengths. [KRT07) .

gradient for Q1 and optimized lengths for Q1, Q2 and Q3. The gap between the quadrupoles is 1 m for the interconnection (a recent study [Par] established that the minimum distance between quadrupoles in two different cryostats is 1.3 m but smaller in case they share the same cryostats). In order to find a suitable collision optics an additional Q6 module has been installed. This layout has been proposed in [BdMO07].

**Modular** This option (see Fig. 5.4.6,) uses a quadruplet design with an intermediate gradient. All the modules have the same length (the name comes from there) but the first two have a larger gradient implying either a reduced aperture for the first two modules or reduced aperture margins in the other modules. The gap between the quadrupoles is 1 m. An advantage of this option is the large set of gaps that can be used for mask absorbers or corrector magnets. In order to find a suitable collision optics an additional Q6 module has been installed. This layout has been proposed in [BdMO07].

**Lowbetamax** This option (see Fig. 5.4.7,) uses a triplet layout and the highest gradient compatible with some additional aperture margin in the triplet. The first element uses a reduced aperture and modules of three different lengths. These choices limit the peak of the beta function in the triplet (the name comes from there). No additional quadrupole modules are installed. This layout has been proposed in [BdMO07].

**Symmetric** This option (see Fig. 5.4.7,) uses a triplet layout and the highest gradient compatible with some additional aperture margin in the triplet. This option uses only two different modules of different length but same aperture and gradient. The modules are arranged almost symmetrically with respect to the center of the triplet assembly (the name comes from there). The gaps are the same with respect to the nominal layout. This triplet layout first appeared in [KRT07].

These options do not cover all the possibilities and should be considered working hypothesis for identifying merits and limitations for the several options in terms of gradient and modularity.

The layout data is summarized in Table 5.1:

For these layouts collision optics with crossing schemes for the entire LHC have been developed. As an example see Fig. 5.4.9.

	Compact	Modular	Lowbetamax	Symmetric
$L^*$ [m]	23	23	24	23
Gradient [T/m]	91,68	115,88,82,84	168,122	122
Module L [m]	12.2,14.6,11	4.8	7.4,5.7,4.9	9.2,7.8
Total L [m]	55	68	40	41
LRBB	23	26	19	19
Aper. MQX [mm]	170,220	130,170	90,130	130
B.S. MQX [mm]	74,79;99,104	54,59;99,104	34,39;54,59	54,59
B.S. D1 [mm]	50,64;45,64	50,64;45,64	50,64;45,64	50,64;45,64

**Table 5.1** Layout parameters for different LHC interaction region layouts. Some layouts that require different gradients and modules lengths. The beam screen apertures are given in term of half gap and radius and for the MQX the two couples refer to the two apertures. The quadrupole apertures were proposed in [BT] . The D1 apertures are proposed in [Far] .

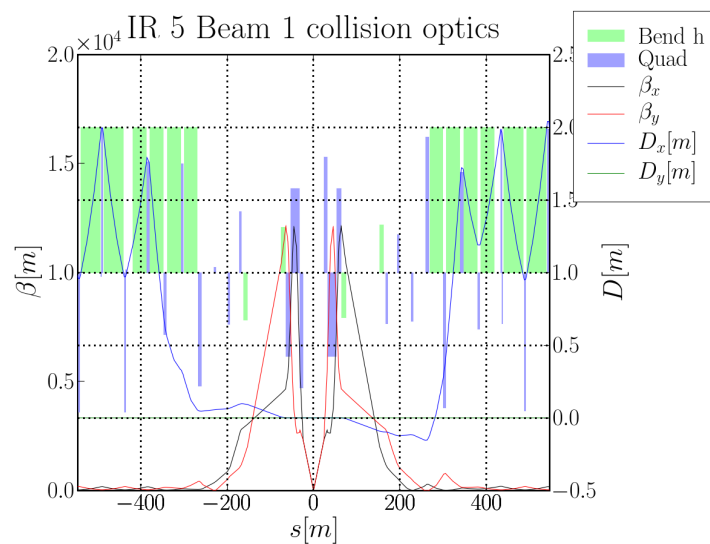


**Figure 5.4.9** Collision optics for Beam 1 in IR 5 for a quadrupole first layouts.



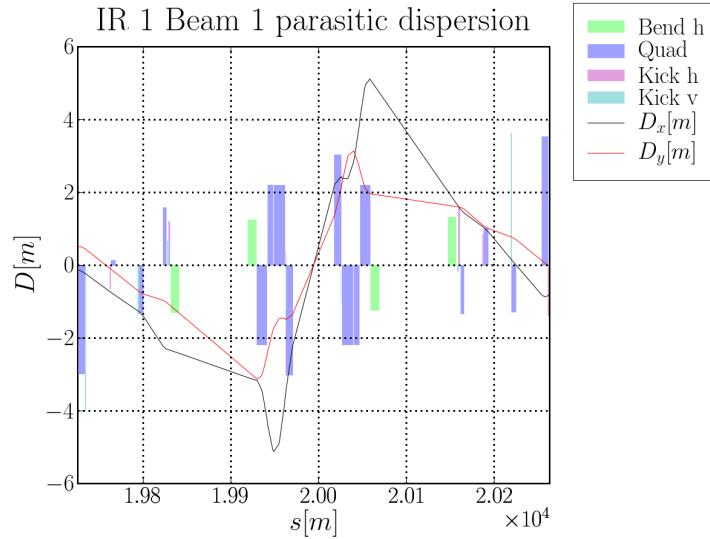


**Figure 5.5.11 Parasitic dispersion Beam 1 in IR 1. The parasitic dispersion generated by the crossing scheme.**

## 5.6 Mechanical aperture

The quantity  $n_1$  (which gives the required distance in sigma of the primary collimator, see [BCL<sup>+</sup>04] and Sec. 3.4.1) has been used for evaluating the aperture margins in the interaction region. The aperture model is indicated for the new elements in Table 5.1. For the rest of the elements the aperture model is the same as the one of the official LHC optics with few exceptions for D2 Q4 and Q5. The aperture of these elements has been optimized for the injection optics with a particular orientation of the beam screen. In case of the upgraded optics the beta functions and as a consequence the crossing scheme pose tighter constraints at collision. The beam screens are consequently rotated in the locations where it is possible to increase aperture margins.

The apertures are computed using closed orbit tolerances of 3 mm, energy spread of  $\delta = 0.00086$  and nominal aperture tolerances. Additional informations are given in [Far07].

The results are summarized in Tab. 5.2 from which it is possible to see that the lower gradient options (Compact and Modular), while offering large aperture margins in the triplet, show aperture bottlenecks in the matching section. The higher gradient options (Lowbetamx and Symmetric), on the contrary, offer a better balance of the aperture margins.

	Compact	Modular	Lowbetamax	Symmetric	LHC
MQX, ap 1	20.026	14.141	7.821	15.466	7.215
MQX, ap 2	16.953	12.633	8.830	8.438	6.845
D1	5.303	6.379	7.607	7.323	7.431
D2	5.372	4.271	7.959	6.518	15.152
Q4	7.387	6.432	8.685	7.184	15.615
Q5	4.701	3.859	10.425	7.028	16.871

Table 5.2 Aperture bottlenecks for the upgrade optics and the nominal LHC in terms of  $n_1$

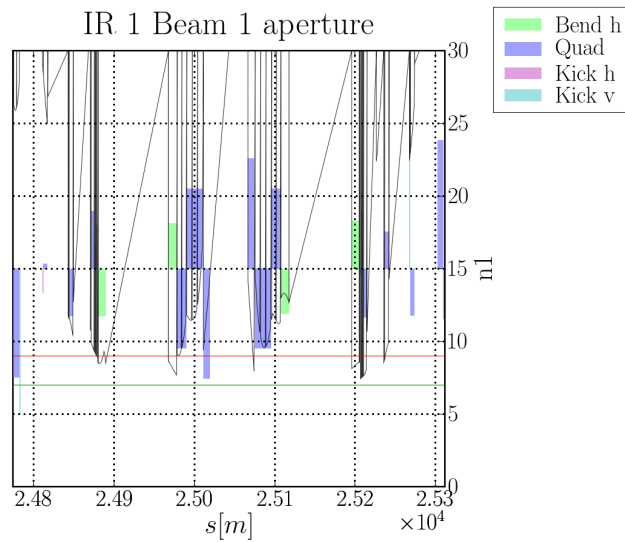
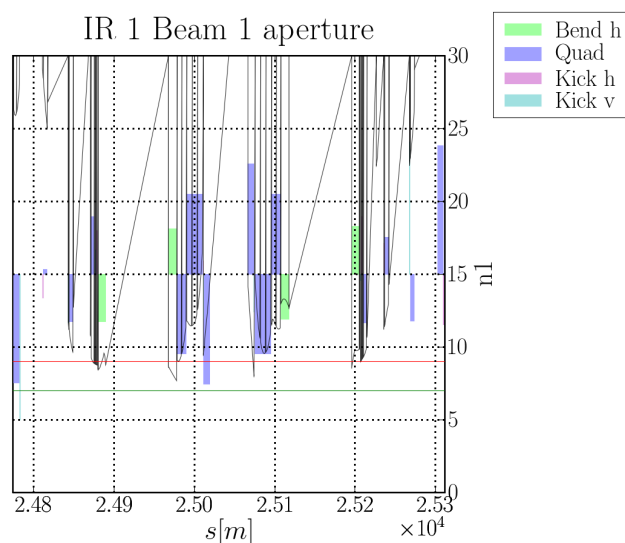


Figure 5.6.12 Aperture for Beam 1 in IR 1 in terms of  $n_1$ .



**Figure 5.6.13** Aperture for Beam 1 in IR 1 in terms of  $n1$  with the beam screen rotated starting from D2. It is possible to note the gain of a aperture margin with respect the non rotated option showed in Fig. 5.6.12.

## 5.7 Chromaticity

The upgrade optics present stronger chromatic effects with respect to the nominal layout due the reduction of  $\beta^*$  which implies a stronger impact of quadrupole errors in the final focusing system.

Table 5.3 shows the values for the required strengths of the arc sextupoles for compensating the first order chromaticity and the off momentum beta beating for two different energy errors.

The results show that, while the natural chromaticity is still correctable by the arc sextupoles, the off momentum beta beat increases by a factor of 3 to 5 with respect to the nominal values. It is not clear whether the rest of the LHC subsystems can cope with such a large beating or if this effect can be corrected while keeping acceptable flexibility in the machine.

## 5.8 Dynamic aperture

In collision the dynamics aperture (DA) is dominated by the non linear fields in the interaction region. The larger contribution to the reduction of DA is the “other” beam which should reduce the DA to  $6\sigma$ .

Another important contribution comes from the field imperfections in

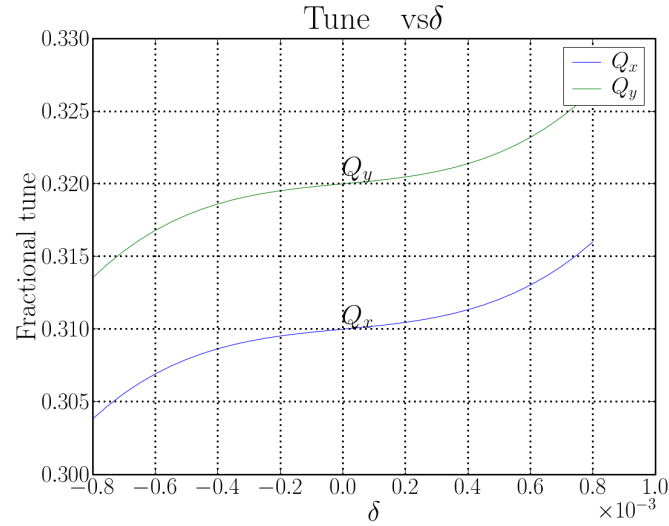


Figure 5.7.14 Chromatic change of the tune for a quadrupole first layout. The non linear terms are much stronger with respect to the nominal values.

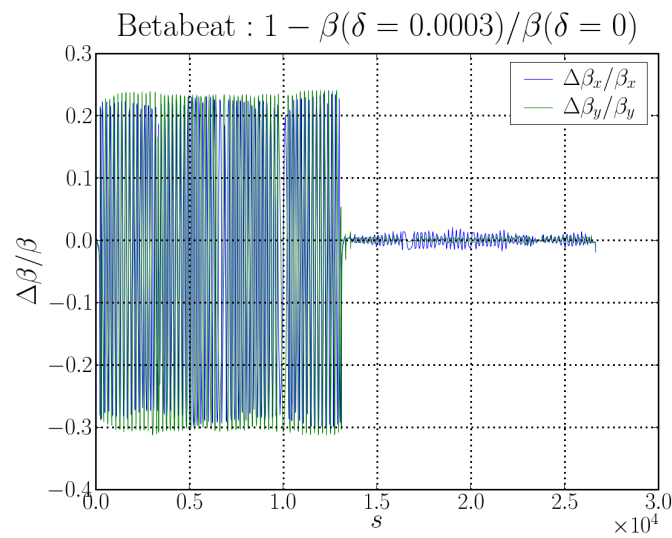


Figure 5.7.15 Chromatic beta-beating at  $\delta = 3 \cdot 10^{-4}$  for a quadrupole first layout. The beta-beating is three times larger with respect to the nominal values.

	Compact	Modular	Lowbetamax	Symmetric	LHC
Sextupoles [%]	88,56	87,58	74,46	75,46	48,28
Beat. $\delta = 3 \cdot 10^{-4}$ [%]	40	40	30	30	10
Beat. $\delta = 8 \cdot 10^{-4}$ [%]	150	150	100	105	30

**Table 5.3 Chromatic aberrations for the upgrade optics and the nominal LHC.** The first row show the required strength of the arc sextupoles for compensating the first order chromaticity, while the last two rows present the off momentum beta beating for two different energy error.

	Compact	Modular	Lowbetamax	Symmetric	LHC
Full	16	11	14	12	12
Triplet only	22	17	14	12	
Triplet excluded	16	11	20	16	

**Table 5.4 Minimum DA over 60 seeds without beam beam effect and field imperfections of D1 and D2.** The second row and the third row show the DA excluding in addition all field imperfections but the triplet and the triplet respectively. The field quality for the triplets is estimated using the results showed in [KRT07].

large beta area (i.e. triplets, D1, D2 and the first elements of the matching section). For the LHC it has been estimated that for preserving the DA to  $6\sigma$  including beam beam, the minimum DA over 60 seeds without beam beam effect should be larger than  $12\sigma$  (see [BCL<sup>+</sup>04]).

In case of the upgrade it is important to design magnets with a field quality that preserve a DA of  $12\sigma$ . Estimates for the field quality of new magnets can be found using the scaling laws presented in [KRT07] and the existing production for the LHC.

Table 5.4 shows the results of the DA studies for the four upgrade optics and the LHC.

Designs with larger aperture margins present larger DA when only triplets error are included. In case of aperture bottlenecks in the matching section, the field quality of those elements starts to be the dominant one. These two facts explain the large differences between the Compact and Modular design with respect to the Lowbetamax and Symmetric. The differences between the Symmetric and Lowbetamax, very similar in terms of field quality, could be explained by the averaging effect of a different number of modules and the uncertainty of the method.

## 5.9 Transition to injection

An optics with  $\beta^* > 5$  m is required at injection because the transverse emittance is four times larger. A set of transition optics should be found in order to change the IR configuration from injection to collision. The quadrupole settings should smoothly change in order to accommodate the restrictions in the power supplies. The transition optics should also have the same phase advance in order to keep the tune of the machine stable.

For the LHC the set of transition optics is hard to find because of the limitations in the maximum current of the magnets and limitations of mechanical aperture in the LSS. Without one of these two limitations it is very straightforward to find a solution because the number of parameters is larger than the number of constraints. The parameters are not truly independent and the solution may or may not exist in case of limitations of aperture, which translates in limitations of the maximum beta in some location, and limitations of quadrupole strengths, which translate in limitations of tunability (roughly proportional to the product  $\beta k$ ).

A preliminary study shows that it is possible to keep the phase advance of the insertion for a large range of  $\beta^*$  only for Lowbetamax and Symmetric.

## 5.10 Conclusion

The development of four different optics showed the actual limitations and challenges for quadrupole first layouts.

The results presented so far show that the Lowbetamax option shows the best overall performance closely followed by the Symmetric option which offers a simpler though less flexible design. Both options can be further optimized to gain aperture margins and represent a good starting point for the final design.

The studies pointed to outstanding issues that need to be further investigated.

Aperture bottlenecks have been identified in D1, D2, Q4, Q5. The limitation in D1 is avoidable and requires a new design for the dipole. The limitations for D2, Q4, Q5 depend on the triplet layout. A further optimization can reduce the problem but on one hand the triplets have a limited number of free parameters to use and on the other hand the LSS is not flexible enough to accept all possible optics functions that merely fulfill the aperture requirements. This limitation is more severe for the Compact and Modular options, while it is presumably fixable for the Symmetric option and barely acceptable for the Lowbetamax option.

The impact of the larger off momentum beta beat and the third order chromaticity need to be studied. It is a global quantity and it may affect other LHC subsystems (e.g. the collimation system).

The presented solution even though it was designed to be as realistic as possible, represents an effort to study the possibilities and implications of several design criteria: gradient and aperture of the quadrupoles, number of modules, triplet or quadruplet design.

The analysis presented is not exhaustive. For a more realistic design many refinements are needed. In particular it is important to check whether the heat load and radiation damage levels are compatible with the new elements and redesign the final focus system for increasing the aperture margins and reserving the right locations for correctors and diagnostics (orbit corrector and BPM).

# Chapter 6

## Conclusions

An upgrade of the LHC interaction regions allows to increase the luminosity by a factor of 1.6 (up to 2) with respect to the nominal performance. The upgrade of the IR affects a limited part of the LHC and it has fewer side effects with respect to other means of increasing the luminosity (e.g. bunch intensity and number of bunches).

The upgrade of the LHC interaction region aims at a reduction of beam transverse size at the IP by reducing  $\beta^*$  from 55 cm to 25 cm. The present IR cannot reach  $\beta^* = 25$  cm because the focus system close to the IP (i.e. triplet) has limitations in the mechanical aperture of the quadrupoles magnet. In addition the present layout is designed to be protected from the debris coming from the IP only for the ultimate luminosity, therefore an upgrade of the luminosity will certainly require a redesign of the particle absorbers.

Being aware of those limitations, two design schemes are proposed and studied, the dipole first layouts and the quadrupole first layouts, which address some of the limitation of the present layout.

The dipole first layouts modify the structure of the present layout and exchange the position of the focusing system and the separation recombination dipoles. The dipoles can act as absorbers because of the spectrometer effect. Their position reduces the number of parasitic interactions between the two beams that is a source of reduction of beam lifetime. This advantages are counterbalanced by the drawbacks of having the focusing system farther from the IP. It implies a growth of the beam size and beta function. The large beta functions are a source of chromatic aberrations, sensitivity to magnet field imperfections and aperture bottlenecks in the matching section. In order to cope with these limitations, the layout studied in the thesis assume magnet parameters at the edge of the theoretical limit of the Nb3Sn technology, currently under active development. Nevertheless the overall performance of the dipole first layout studied in the thesis proved that the implementation

is still challenging.

Quadrupole first layouts represent instead a viable option for an upgrade. A quadrupole first layout does not imply a change of the structure of the interaction region, but an optimization of the focus system. It has been assumed that the magnet should use NbTi magnets, the technology used in the LHC that is proved feasible as of today in order to design options that are practically realizable. In this case the challenge is to find options with better performance as compared to the nominal LHC using the same technology. The only difference is an increase of experience in manufacturing NbTi magnets, as compared to the one at the time the LHC was designed. The thesis shows the development of an analytical method that allows to find the intrinsic limitations of a focusing system. Using this information, together with the limitations of the NbTi technology and the one coming from the beam dynamics, it is possible to define a region of parameters that fulfill the requirements of the upgrade and are compatible with the existing technology. The analytical method gives also indications on how to construct optimized layouts and it has been used to design and study realistic implementations of quadrupole first layouts. In particular it was possible to demonstrate that longer and weaker quadrupoles allow a reduction of the transverse beam size at the IP and at the same time an increase of the aperture margins.

The implementations address several design criteria such as large aperture margins for extending the flexibility and reducing the energy deposited in the magnet coils, modular design to reduce the number of spares magnet and therefore the overall cost of the upgrade and finally reducing the intrinsic aberrations and avoid aperture bottlenecks in the matching section. The analysis showed that some of the options require additional changes in the matching section, while others reach the upgrade goals by changing a limited number of quadrupoles.

These results contributed to the approval of a CERN project that aims at bringing the LHC to ultimate performance by implementing a low gradient quadrupole first layout.

# Appendix A

## Optimization tools for accelerator optics

### A.1 Introduction

A new matching algorithm and a new matching mode have been developed and implemented for MadX [SIG]. The new algorithm, called JACOBIAN, is able to solve a generalized matching problem with an arbitrary number of variables and constraints. It aims at solving the corresponding least square problem. The new mode, called USE\_MACRO, allows the user to construct his own macros and expressions for the definition of the constraints in a matching problem. The new algorithm combined with the macro constructs was successfully used for finding optic transitions and a non-linear chromaticity correction. This new approach can be seen as a major upgrade of the matching capabilities of MadX taking advantage of various modules like TWISS, PTC, TRACK, SURVEY, APERTURE, and so on.

MadX provides several other matching algorithms:

- LMDIF: fast but limited to problems where the number of variables is not greater than the number of constraints and the constraints are differentiable,
- SIMPLEX: suited for problems where the constraints are differentiable, slower than LMDIF, not always suited for constrained problems for which solutions tend to go far from the starting point;

The new matching routines JACOBIAN has been developed in order to provide solutions for:

- problems for an arbitrary number of variables and constraints,

- constrained problems where it is interesting to find the closest solution from the starting point,
- constraints on the variation of a variable (see SLOPE option in VARY command [SIG]);

MadX can match quantities calculated by the twiss command and stored in the TWISS or SUMM table. A new mode USE\_MACRO has been developed to let the user define its own observables using all available MadX modules.

## A.2 Optimization and least-sqaure fitting

An optimization problem can be written as:

$f(x)$  A function  $\mathbb{R}^n : \mathbb{R}$  to be minimized

$c_i(x) = 0, i \in \mathcal{E}$  A set of equalities to be fulfilled

$c_i(x) \geq 0, i \in \mathcal{I}$  A set of inequalities to be fulfilled

The function  $f$  can be expanded in Taylor series, therefore

$$f(x+p) = f(x) + \nabla f(x+tp)^T p \quad t \in [0, 1] \quad (\text{A.2.1})$$

$$f(x+p) = f(x) + \nabla f(x)^T p + \frac{1}{2} p^T \nabla^2 f(x+tp) p \quad t \in [0, 1]. \quad (\text{A.2.2})$$

$x^*$  is local minimizer if

$$\nabla f(x^*) = 0 \quad \nabla^2 f(x^*) \text{ positive semidefinite} \quad (\text{A.2.3})$$

A set  $S$  is convex if for every  $x, y \in S, \alpha x + (1-\alpha)y \in S$  for all  $\alpha \in [0, 1]$ . A function  $f$  is convex if for every  $x, y \in S, f(\alpha x + (1-\alpha)y) \leq \alpha f(x) + (1-\alpha)f(y)$  for all  $\alpha \in [0, 1]$ .

If a function is convex a local minimizer is also a global minimizer.

A least square problem is defined if  $f$  is

$$f(x) = \frac{1}{2} \sum r_i(x)^2 = \frac{1}{2} |r(x)|^2 \quad (\text{A.2.4})$$

If  $J(x) = \frac{\partial r_i}{\partial x_j}$  is the Jacobian then

$$\nabla f(x) = J(x)^T r(x) \quad \nabla^2 f(x) = J(x)^T J(x) + r(x)^T \nabla^2 r(x) \quad (\text{A.2.5})$$

If  $r(x)$  are linear

$$x^* = \sum_{\sigma_i \neq 0} \frac{u_i^T r}{\sigma_i} v_i + \sum_{\sigma_i = 0} \tau_i v_i \quad (\text{A.2.6})$$

If  $\tau_i = 0$  then  $x^*$  is the solution which minimizes  $|x^*|$ .

### A.3 Singular value decomposition

A  $m \times n$  rectangular matrix  $M$  can always be decomposed in

$$M = U \Sigma V^* \quad (\text{A.3.1})$$

where  $U$  is a  $m \times m$  matrix,  $\Sigma$  is a  $m \times n$  diagonal matrix and  $V$  is a  $n \times n$  matrix.

If  $M$  is a linear transformation  $a \xrightarrow{M} b$  the following commutative diagram applies:

$$\begin{array}{ccc} a & \xrightarrow{M} & b \\ \downarrow V & & \downarrow U \\ \alpha & \xrightarrow{\Sigma} & \beta \end{array} \quad (\text{A.3.2})$$

If  $v_i$  is the  $i$ th column of  $V$ ,  $\sigma_i$  is the  $i$ th element of the  $\Sigma$  diagonal and  $u_i$  the  $i$ th column of  $U$  then

$$b = \sum_i u_i \sigma_i v_i^* a \quad (\text{A.3.3})$$

or

$$M v_i = \sigma_i u_i \quad (\text{A.3.4})$$

The pseudo inverse of  $M$  can be calculated by:

$$M^{-1} = V \Sigma^+ U^* \quad (\text{A.3.5})$$

$$M_{ij}^{-1} = \sum_{t=1}^{\min(n,m)} V_{it} \frac{1}{S_{tt}} U_{tj}, \quad (\text{A.3.6})$$

where  $\Sigma^+$  is  $\Sigma^*$  with nonzero entries replaced by their reciprocal.

If the singular values are sorted in crescent order and  $s$  is the index of the last non-zero singular value then:

- $u_1, \dots, u_s$  span the range of  $M^{-1}$
- $u_{s+1}, \dots, u_m$  span the null space of  $M^{-1}$
- $v_1, \dots, v_s$  span the range of  $M$
- $v_{s+1}, \dots, v_n$  span the null space of  $M$

## A.4 JACOBIAN algorithm

### Algorithm

The algorithm is based on the Newton-Raphson method.

A matching problem can be defined as

$$\mathbf{c} = \mathbf{f}(\mathbf{v})$$

where  $\mathbf{c}$  is the vector of the  $c$  constraints,  $\mathbf{v}$  is the vector of the  $v$  variables and  $\mathbf{f}$  is vector field representing accelerator quantities.

If  $\mathbf{c}_0 = \mathbf{f}(\mathbf{v}_0)$  is a solution for  $\mathbf{c}_0$  close to  $\mathbf{c}$  then

$$\mathbf{c} = \mathbf{c}_0 + \frac{D\mathbf{f}}{D\mathbf{v}}(\mathbf{v}_0)\delta\mathbf{v} + O(|\delta\mathbf{v}|^2)$$

and the solution can be found by iterating the equations:

$$\mathbf{v} = \mathbf{v}_0 + \alpha_n \delta\mathbf{v} \quad \frac{D\mathbf{f}}{D\mathbf{v}} = \mathbf{J} \quad \delta\mathbf{v} = \mathbf{J}^{-1}(\mathbf{c} - \mathbf{c}_0).$$

where  $\mathbf{J}$  is the Jacobian of the transformation,  $\delta\mathbf{v}$  is the vector which points to the solution,  $\alpha_n$  is the succession  $2^{-n}$  and  $n$  is chosen such that the penalty function  $|\mathbf{c} - \mathbf{c}_0|$  is smaller than the one of the previous step (see BISEC in [SIG]).

If  $\mathbf{J}$  is a  $c \times v$  matrix and  $c = v$ , the system can be solved exactly, if  $v > c$  or  $v < c$  is solved by a QR or LQ decomposition [ABB<sup>+</sup>99] yielding the minimization of  $|\mathbf{c} - \mathbf{c}_0|$  or  $|\delta\mathbf{v}|$  respectively.

If a constraint is an inequality:

- it's removed from the system when it is fulfilled,
- otherwise it is treated as an equality.

At each iteration step, if a variable it is assigned out of its boundaries:

- if  $v > c$  the variable is excluded from the set and linear system is solved again,
- if  $v = c$  or there were too many exclusions the variable is reseted to its limit (see **STRATEGY** in [SIG]).

In addition, before the matching process, the following transformation can be applied to variable vector:

- a uniform random vector is added to the variables (see **RANDOM** in [SIG]) in order to avoid local minima;
- the variables are moved towards a desired value (see **COOL**, **BALANCE**, **OPT** in [SIG]) in order to force the final solution.

Figure 1 shows the scheme of the algorithm.

## USE\_MACRO

The new mode is based on the idea that:

- the constraints can be user defined expressions,
- the calculations for evaluating these expressions can be defined via macros.

In this way, every quantity which can be calculated via macros and expressions can be accessed by the user and be used by the matching algorithm.

The expressions can contain algebraic functions of values from the MadX tables through the **TABLE** construct.

The syntax is slightly different from the old style matching and has 2 variants:

- using an already defined macro

```
m1: macro= {y=(x-3.5)*(x+2)*(x-4); };
match,use_macro;
  vary,name=x;
  use_macro: name= m1;
  constraint,expr= y=0;
  jacobian,tolerance=1.e-24;
endmatch;
```

- or an implicit definition of the macro

```

match,use_macro;
  vary,name=x;
  m1: macro= {y=(x-3.5)*(x+2)*(x-4); };
  constraint,expr= y=0;
  jacobian,tolerance=1.e-24;
endmatch;

```

More than one set of macros and constraints can be specified in sequence:

```

match,use_macro;
  vary,name=x;
  m1: macro= {y=(y-3.5)*(x+2)*(x-4); };
  constraint,expr= y=0;
  m2: macro= {y=(y-3.5)*(x-1.4)*(x+3.5); };
  constraint,expr= y=0;
  jacobian,tolerance=1.e-24;
endmatch;

```

## Real life example

This example shows the correction of the first and second order chromaticity in a LHC IR upgrade option using all the available sextupoles families independently.

```

madchrom: macro={
  twiss;
  qx0=table(summ,q1);
  qx1=table(summ,dq1);
  qy0=table(summ,q2);
  qy1=table(summ,dq2);
  dpp=.00001;
  twiss,deltap=dpp;
  qxpp=table(summ,q1);
  qypp=table(summ,q2);
  twiss,deltap=-dpp;
  qxmp=table(summ,q1);
  qymp=table(summ,q2);
  qx2=(qxpp-2*qx0+qxmp)/dpp^2;

```

```

    qy2=(qypp-2*qy0+qymp)/dpp^2;
};

use,sequence=lhcb1;
match,use_macro;
vary, name=ksd1.a12b1; vary, name=ksd1.a23b1;
vary, name=ksd1.a34b1; vary, name=ksd1.a45b1;
vary, name=ksd1.a56b1; vary, name=ksd1.a67b1;
vary, name=ksd1.a78b1; vary, name=ksd1.a81b1;
vary, name=ksd2.a12b1; vary, name=ksd2.a23b1;
vary, name=ksd2.a34b1; vary, name=ksd2.a45b1;
vary, name=ksd2.a56b1; vary, name=ksd2.a67b1;
vary, name=ksd2.a78b1; vary, name=ksd2.a81b1;
vary, name=ksf1.a12b1; vary, name=ksf1.a23b1;
vary, name=ksf1.a34b1; vary, name=ksf1.a45b1;
vary, name=ksf1.a56b1; vary, name=ksf1.a67b1;
vary, name=ksf1.a78b1; vary, name=ksf1.a81b1;
vary, name=ksf2.a12b1; vary, name=ksf2.a23b1;
vary, name=ksf2.a34b1; vary, name=ksf2.a45b1;
vary, name=ksf2.a56b1; vary, name=ksf2.a67b1;
vary, name=ksf2.a78b1; vary, name=ksf2.a81b1;
use_macro,name=madchrom;
constraint,expr= qx1=2;
constraint,expr= qy1=2;
constraint,expr= abs(qx2)<2;
constraint,expr= abs(qy2)<2;
jacobian,calls=10,bisec=3;
endmatch;

```

This problem is solved by JACOBIAN in 5 iteration for a total of 160 calls of the macro. The problem could also be solved by the SIMPLEX method but solution doesn't converge. Reducing the number of variables to 4 in order to use LMDIF brings to a solution which requires 50% more strength for the sextupoles because JACOBIAN, via the LQ decomposition, solve the least square problems in the iterations.

## A.5 Conclusion

The JACOBIAN procedure combined with the USE\_MACRO construct has been successfully used for finding smooth optics transitions, estimation of the

tunability of insertion regions ([SSdMF06]) and for non-linear chromaticity correction([dMBR06],[dMB06]).

JACOBIAN performs better than the other methods in case that

- the problem is almost linear and the constraints are differentiable;
- the starting point is close to the solution;
- the problem is such that  $v > c$ ;

otherwise SIMPLEX or LMDIF provide better results, for problems in which the constraints are not differentiable or differentiable respectively.

USE\_MACRO extends the optimization capabilities for linear and non-linear optics, aperture, tracking, resonant driving terms and so on.

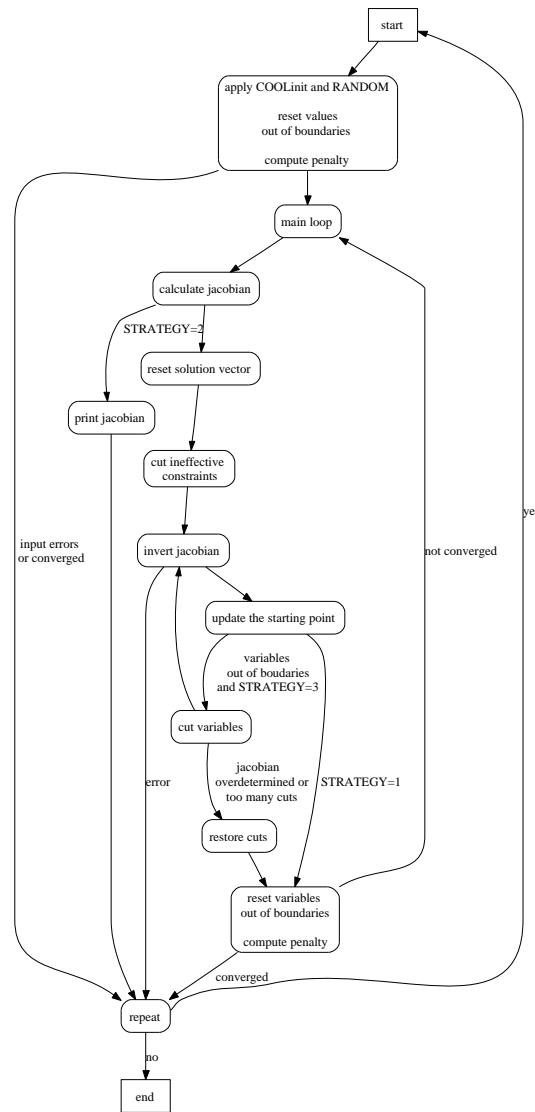


Figure A.4.1 Algorithm of JACOBIAN



# Bibliography

- [ABB<sup>+</sup>99] E. Anderson, Z. Bai, C. Bischof, S. Blackford, J. Demmel and J. Dongarra, J. Du Croz, A. Greenbaum, S. Hammarling, A. McKenney, and D. Sorensen. *LAPACK Users' Guide Third Edition*. 1999.
- [BC07] O. Bruening and P. Collier. Building a behemoth. *Nature*, 448, jul 2007.
- [BCG<sup>+</sup>02] Oliver Sim Bruening, Roberto Cappi, R. Garoby, O. Groebner, W. Herr, T. Linnecar, R. Ostojic, K. Potter, L. Rossi, F. Ruggiero, Karlheinz Schindl, Graham Roger Stevenson, L. Tavian, T. Taylor, Emmanuel Tsesmelis, E. Weisse, and Frank Zimmermann. LHC luminosity and energy upgrade : A feasibility study. Technical Report LHC-Project-Report-626, CERN, December 2002.
- [BCL<sup>+</sup>04] O. Bruening, P. Collier, P. Lebrun, S. Myers, R. Ostojic, J. Poole, and P. Proudlock. LHC design report. Technical Report CERN-2004-003, CERN, 2004.
- [BdM07] O. Bruening and R. de Maria. Low gradient triplet layout options. In *3rd CARE-HHH-APD Workshop: Towards a Roadmap for the Upgrade of the LHC and GSI Accelerator Complex LHC-LUMI-06*, 2007.
- [BdMO07] O. Bruening, R. de Maria, and R. Ostojic. Low gradient, large aperture ir upgrade options for the lhc compatible with nb-ti magnet technology. LHC-Report 1008, CERN, jun 2007.
- [BFMG04] O. Bruening, S. Fartoukh, and T. Risselada M. Giovannozzi. Dynamic aperture studies for the lhc separation dipoles. Technical Report LHC-Project-Note-349., CERN, Geneva, Jun 2004.

## Bibliography

---

- [BKT07] B. Bellesia, J. Koutchouk, and E. Todesco. Field quality in low-beta superconducting quadrupoles and impact on the beam dynamics for the large hadron collider upgrade. *PRSTAB*, 10(062401):8, jan 2007.
- [Bru99] O. Bruening. Optics solutions in ir1 and ir5 for ring-1 and ring-2 of the lhc version 6.0. Technical Report CERN-LHC-Project-Note-187, CERN, April 1999.
- [Bru05] O. Bruening. Possible dipole first options and challenges, September 2005. LHC LUMI 2005 CARE-HHH-APD Workshop.
- [BS84] Karl L. Brown and Roger V. Servranckx. First and second order charged particle optics. Technical Report SLAC-PUB-3381, SLAC, July 1984.
- [BS87] Karl L. Brown and Roger V. Servranckx. Optics modules for circular accelerator design. *Nuclear Instruments and Methods in Physics Research Section A: Accelerators, Spectrometers, Detectors and Associated Equipment*, 258(3):480–502, August 1987.
- [BT] F. Borgnolutti and E. Todesco. Quadrupole design for quadrupoles based on lhc nb-ti cables. Private communication.
- [Cha93] W. Chao. *Physics of collective beam instabilities in high energy accelerators*. Wiley, New York, NY, 1993.
- [CS58] E. D. Courant and H. S. Snyder. Theory of the alternating-gradient synchrotron. *Annals of Physics*, 1(3):1–48, jan 1958.
- [CT99] A. Chao and M. Tigner. *Handbook of accelerator physics and engineering*. World Scientific, Singapore, 1999.
- [CTZ07] R Calaga, R Tomás, and F Zimmermann. Crab cavity option for lhc ir upgrade. In *3rd CARE-HHH-APD Workshop: Towards a Roadmap for the Upgrade of the LHC and GSI Accelerator Complex, IFIC, Valencia, Spain, 16 - 20 Oct 2006*, page 7 p, 2007.
- [dG97] E. T. d’Amico and G. Guignard. Analysis of a symmetric triplet and its application to ring insertions. CLIC-Note 341, CERN, May 1997.

## Bibliography

---

- [dG98] E.T. d’Amico and G. Guignard. Analysis of generic insertions made of two symmetric triplets. CERN-SL 98-014, CERN, May 1998.
- [dM05] R. de Maria. LHC IR upgrade: a dipole first option. In *2nd CARE-HHH-ADP Workshop on Scenarios for the LHC Luminosity Upgrade LHC-LUMI-05*, pages 33–39, September 2005.
- [dM07a] R. de Maria. Layout design for final focus systems and applications for the lhc interaction region upgrade. LHC-Report 1051, CERN, sep 2007.
- [dM07b] R. de Maria. Lhc ir upgrade: Dipole first with chromaticity and dynamic aperture issues. In *3rd CARE-HHH-APD Workshop: Towards a Roadmap for the Upgrade of the LHC and GSI Accelerator Complex LHC-LUMI-06*, 2007.
- [dMB06] R. de Maria and O. Bruening. A low gradient quadrupole first layout compatible with nbt magnet technology and  $\beta^* = 0.25\text{m}$ . Technical Report CERN-LHC-Project-Report-933, CERN, June 2006. Presented at: European Particle Accelerator Conference EPAC’06 , Edinburgh, Scotland, UK , 26 - 30 Jun 2006.
- [dMBR06] R. de Maria, O. Bruening, and P. Raimondi. LHC IR upgrade: A dipole first option with local chromaticity correction. Technical Report CERN-LHC-Project-Report-934, CERN, June 2006. Presented at: European Particle Accelerator Conference EPAC’06 , Edinburgh, Scotland, UK , 26 - 30 Jun 2006.
- [dMSS06] R. de Maria, F. Schmidt, and P. K. Skowronski. Advances in matching with mad-x. In *Proceedings of ICAP*, September 2006.
- [dMT] R. de Maria and R. Tomas. Web repository of ir upgrade options. [http://care-hhh.web.cern.ch/CARE-HHH/SuperLHC\\_IROptics/IRoptics.html](http://care-hhh.web.cern.ch/CARE-HHH/SuperLHC_IROptics/IRoptics.html).
- [DZ07] U Dorda and F Zimmermann. Long-range beam-beam compensation with wires. In *3rd CARE-HHH-APD Workshop: Towards a Roadmap for the Upgrade of the LHC and GSI Accelerator Complex, IFIC, Valencia, Spain, 16 - 20 Oct 2006*, page 3 p, 2007.

## Bibliography

---

- [DZFS] U Dorda, F Zimmermann, W Fischer, and V Shiltsev. Lhc beam-beam compensation using wires and electron lenses. In *PAC07*.
- [Egg04] K. Eggert. Total cross-section, elastic scattering and diffraction dissociation at the large hadron collider at cern: Totem design report. Cern-lhcc-2004-002, CERN, January 2004.
- [Far] S. Fartoukh. Lss magnet aperture requirements. Presented at LIUWG in 27.09.2007.
- [Far99] Stephane Fartoukh. Second order chromaticity correction of LHC v6.0 at collision. Technical Report cern-lhc-project-report-308, CERN, October 1999.
- [Far07] S. Fartoukh. Lss magnet aperture requirements for the lhc insertion upgrade, a first estimate. Technical Report LHC-PROJECT-Report-1050, CERN, oct 2007.
- [Far09] S. Fartoukh. Prospective for flat beam optics. Presented at LHC MAC 15-17 June 2009, 2009.
- [FGdMG07] A. Faus-Golfe, R. de Maria, and R. Tomas Garcia. Limits on chromaticity correction. In *3rd CARE-HHH-APD Workshop: Towards a Roadmap for the Upgrade of the LHC and GSI Accelerator Complex LHC-LUMI-06*, 2007.
- [GAG<sup>+</sup>05] R. C. Gupta, M. Anerella, A. Ghosh, M. Harrison, J. Schmalzle, P. Wanderer, and N. V. Mokhov. Optimization of open mid-plane dipole design for LHC IR upgrade. *Particle Accelerator Conference (PAC 05)*, May 2005.
- [Gia99] F. Gianotti. Collider physics: Lhc. Atlas note 2000-001, CERN, sep 1999.
- [GMV02] F. Gianotti, M. L. Mangano, and T. Virdee. Physics potential and experimental challenges of the lhc luminosity upgrade. CERN-TH CERN-TH-2002-078, CERN, apr 2002.
- [HM03] W. Herr and B. Muratori. Concept of luminosity. In *CAS - Intermediate Course on Accelerator Physics, DESY, Zeuthen, Germany, 15 - 26 Sep 2003*, 2003.

## Bibliography

---

- [JO97] J. B. Jeanneret and R. Ostojic. Geometrical acceptance in LHC version 5.0. CERN-LHC-Project-Note 111, CERN, September 1997.
- [KAM<sup>+</sup>07] J-P. Koutchouk, R. Assmann, E. Métral, E. Todesco, F. Zimmermann, R. de Maria, and G. Sterbini. A concept for the lhc luminosity upgrade based on strong beta\* reduction combined with a minimized geometrical luminosity loss factor. In *Proceedings of PAC07, Albuquerque, New Mexico, USA, 2007*.
- [KRT07] J. P. Koutchouk, L. Rossi, and E. Todesco. A solution for phase-one upgrade of the LHC low-beta quadrupoles based on nb-ti. lhc-project-report 1000, CERN, April 2007.
- [Mok05] Nikolai Mokhov. Energy deposition in midplane dipole. In *LARP Collaboration Meeting 4*, April 2005. Talk.
- [Ohm05] K Ohmi. Study of crab cavity option for lhc. In *1st CARE-HHH-APD Workshop on Beam Dynamics in Future Hadron Colliders and Rapidly Cycling High-Intensity Synchrotrons, CERN, Geneva, Switzerland, 8 - 11 Nov 2004*, 2005.
- [Par] V. Parma. Space constraints for the triplet cryostats. Presented at LIUWG in 18.10.2007.
- [Peg84] S. Peggs. Minimising chromaticity in interaction regions with long weak quadrupoles. In *SSC Summer Study*, 1984.
- [Reg67a] E. Regenstreif. Phase-space transformations by means of quadrupole multiplets. CERN 67-6, CERN, March 1967.
- [Reg67b] E. Regenstreif. Possible and impossible phase-space transformations by means of alternating-gradient doublets and triplets. CERN 67-8, CERN, March 1967.
- [RS01] P. Raimondi and Andrei Seryi. Novel final focus design for future linear colliders. *Phys. Rev. Lett.*, 86(17):3779 – 3782, apr 2001.
- [SIG] F. Schmidt, G. Iselin, and H. Grote. Madx manual. <http://cern.ch/mad/>.
- [SJM<sup>+</sup>06] T Sen, J Jstone, Nikolai Mokhov, W Fischer, Ramesh Gupta, and Ji Qiang. Us-larp progress on lhc ir upgrades. In *2nd*

## Bibliography

---

- CARE-HHH-APD Workshop on Scenarios for the LHC Luminosity Upgrade, Arcidosso, Italy, 31 Aug - 3 Sep 2005*, 2006.
- [SJRT07] T Sen, J Jstone, V Ranjibar, and R Tomas. Ir upgrade with quadrupoles first and dipoles first. In *3rd CARE-HHH-APD Workshop: Towards a Roadmap for the Upgrade of the LHC and GSI Accelerator Complex, IFIC, Valencia, Spain, 16 - 20 Oct 2006*, page 6 p, 2007.
- [SSdMF06] P. K. Skowronski, F. Schmidt, R. de Maria, and E. Forest. New developments of mad-x using ptc. In *Proceedings of ICAP 2006*, September 2006.
- [SSM05] T Sen, J Strait, and N Mokhov. Overview of possible lhc ir upgrade layouts. In *1st CARE-HHH-APD Workshop on Beam Dynamics in Future Hadron Colliders and Rapidly Cycling High-Intensity Synchrotrons, CERN, Geneva, Switzerland, 8 - 11 Nov 2004*, 2005.
- [TdMZ07] R. Tomas, R. de Maria, and F. Zimmermann. Crab cavity ir optics design with  $t=8\text{mrad}$ . In *3rd CARE-HHH-APD Workshop: Towards a Roadmap for the Upgrade of the LHC and GSI Accelerator Complex LHC-LUMI-06*, 2007.
- [Tüc07] J Tückmantel. Technological aspects of crab cavities. In *3rd CARE-HHH-APD Workshop: Towards a Roadmap for the Upgrade of the LHC and GSI Accelerator Complex, IFIC, Valencia, Spain, 16 - 20 Oct 2006*, page 6 p, 2007.
- [Zie95] Volker Ziemann. Crude scaling laws for the dynamic aperture of LHC from random non-linear errors. Technical Report CERN-SL-Note-95-20-AP, CERN, February 1995.
- [Zim05] F Zimmermann. Beam-beam compensation schemes. In *1st CARE-HHH-APD Workshop on Beam Dynamics in Future Hadron Colliders and Rapidly Cycling High-Intensity Synchrotrons, CERN, Geneva, Switzerland, 8 - 11 Nov 2004*, 2005. Fulltext not available.
- [Zim08] F. Zimmermann. Cern task force on lhc luminosity and energy upgrade, organized by francesco ruggiero, 1st meeting 03.07.2001, 2008. private communication.

## Bibliography

---

- [ZK06] A V Zlobin and V Kashikhin. Study of 2-in-1 large-aperture nb3sn ir quadrupoles for the lhc luminosity upgrade. In *EPAC06*, page 3 p, 2006.

## Bibliography

---

# Curriculum Vitae

## Riccardo de Maria

### Personal Data

First name Riccardo  
Family name de Maria  
Address Brookhaven National Laboratory  
Bldg 902A, 11973, Upton, NY, USA.  
Telephones +41 328 746 1346 (Mobile)  
E-Mail riccardo.de.maria@cern.ch  
Place and Date of Birth Rome, Italy, December 19, 1977  
Nationality Italian  
Compulsory Military Service Done

### Education

2008 PhD at the École Polytechnique fédérales in Lausanne.  
Thesis: “LHC Interaction Region Upgrade”.

2004 “Laurea” degree (five years master course), in Electrical  
Engineering at “La Sapienza” University of Rome, Italy.  
Thesis at CERN: “Time Transient Effects in Superconducting  
Magnets”. Grade: summa cum laude.

2003 “JUAS Accelerator Physics and Accelerator Technologies  
Diploma”, Archamps, France. Grade and ranking respec-  
tively: A, 3<sup>rd</sup>/16; A, 1<sup>st</sup>/20.

1996 High School Degree “Maturità Scientifica”, at “Liceo Scien-  
tifico Statale Nomentano”, Rome, Italy. Grade: 54/60.

### Work Experiences

2008-Today “Toohig” distinguished fellowship at Brookhaven National  
Laboratory, Upton, NY. Supervisor Dr. Steve Peggs.

2005-2008 Doctoral Student at CERN, Accelerator and Beam Depart-  
ment, in accelerator beam optics. Subject: “LHC Luminos-  
ity Upgrade”. Supervisor: Dr. Oliver Brüning.

2004 Technical Student at CERN, Accelerator Technologies De-  
partment, in numerical field computation. Laurea Degree  
Thesis : “Transient Time Effects in Superconducting Mag-  
nets”. Supervisor: Dr. Stephan Russenschuck.

1998–2000 Fellowship at “Dipartimento di Energetica”, “La Sapienza”  
University of Rome, during which I make assistance in us-  
ing didactic software, development and presentation of  
physics didactic experiences.  
Supervisor: Prof. Luigi Palumbo.

## Other Experiences

2001–2003 Student representative at “La Sapienza” University of Rome.  
7/1999–10/2000 Compulsory military service.

## Honors

2004 EPAC 2004 Grant as outstanding student at JUAS.  
1998 and 1999 Fellowship at “Dipartimento di Energetica” at “La Sapienza” University of Rome, Italy.

## Research Activities

Beam dynamics and beam optics ( [1], [2], [3], [4], [5], [6], [7], [8], [9], [10], [11], [12] )

Electromagnetic modeling of superconducting magnets ( [13], [14] [15], [16] )

Computer codes for beam dynamics and beam optics ( [17], [18] )

Vibration measurements and data acquisition ( [19] )

Optimization algorithms ( [18] )

## Skills

Numerical computation programming in Fortran (90,77) C/C++, Python. High performance linear algebra routines (BLAS, LAPACK, MKL). Computer algebra and numerical software (Mathematica, Matlab and similar).

Design tool for magnet design and particle dynamics.

Scientific instrumentation for electronics and electromagnetic fields (oscilloscope, network analyzer, digitizer), data acquisition (LabView, custom development with GPIB, VXI11).

Generic programming also in Java, Perl, Bash. Development mainly in Unix environments.

Experience in electronic design, control systems and RF engineering.

## Foreign Languages

Italian Mother Tongue.  
English Fluent in writing and speaking.  
French Good.

Rome, June 16, 2008

## References

- [1] R. de Maria. Layout design for final focus systems and applications for the lhc interaction region upgrade. LHC-Report 1051, CERN, sep 2007.
- [2] O. Bruening, R. de Maria, and R. Ostojic. Low gradient, large aperture ir upgrade options for the lhc compatible with nb-ti magnet technology. LHC-Report 1008, CERN, jun 2007.
- [3] O. Bruening and R. de Maria. Low gradient triplet layout options. In *3rd CARE-HHH-APD Workshop: Towards a Roadmap for the Upgrade of the LHC and GSI Accelerator Complex LHC-LUMI-06*, 2007.
- [4] R. de Maria. Lhc ir upgrade: Dipole first with chromaticity and dynamic aperture issues. In *3rd CARE-HHH-APD Workshop: Towards a Roadmap for the Upgrade of the LHC and GSI Accelerator Complex LHC-LUMI-06*, 2007.
- [5] R. Tomas, R. de Maria, F. Ruggiero, and F. Zimmermann. Lhc upgrade ir optics web repository. In *3rd CARE-HHH-APD Workshop: Towards a Roadmap for the Upgrade of the LHC and GSI Accelerator Complex LHC-LUMI-06*, 2007.
- [6] R. Tomas, R. de Maria, and F. Zimmermann. Crab cavity ir optics design with  $\tau=8\text{mrad}$ . In *3rd CARE-HHH-APD Workshop: Towards a Roadmap for the Upgrade of the LHC and GSI Accelerator Complex LHC-LUMI-06*, 2007.
- [7] J-P. Koutchouk, R. Assmann, E. Métral, E. Todesco, F. Zimmermann, R. de Maria, and G. Sterbini. A concept for the lhc luminosity upgrade based on strong  $\beta^*$  reduction combined with a minimized geometrical luminosity loss factor. In *Proceedings of PAC07, Albuquerque, New Mexico, USA*, 2007.
- [8] A. Faus-Golfe, R. de Maria, and R. Tomas Garcia. Limits on chromaticity correction. In *3rd CARE-HHH-APD Workshop: Towards a Roadmap for the Upgrade of the LHC and GSI Accelerator Complex LHC-LUMI-06*, 2007.
- [9] R. de Maria and O. Bruening. A low gradient quadrupole first layout compatible with nbti magnet technology and  $\beta^*=0.25\text{m}$ . Technical Report CERN-LHC-Project-Report-933, CERN, June 2006. Presented at: European Particle Accelerator Conference EPAC'06 , Edinburgh, Scotland, UK , 26 - 30 Jun 2006.
- [10] R. de Maria, O. Bruening, and P. Raimondi. LHC IR upgrade: A dipole first option with local chromaticity correction. Technical Report CERN-LHC-Project-Report-934, CERN, June 2006. Presented at: European Particle Accelerator Conference EPAC'06 , Edinburgh, Scotland, UK , 26 - 30 Jun 2006.
- [11] M. Giovannozzi, R. de Maria, S. Fartoukh, S. Gilardoni, J.-B. Jeanneret, A. Lombardi, Y. Papaphilippou, and T. Risselada. Dynamical aperture studies for the cern lhc: Comparison between statistical assignment of magnetic field errors and actual measured field errors. In *Proceedings of EPAC 2006, Edinburgh, Scotland*, 2006.

- [12] R. de Maria. A general method for final focus system design for circular colliders. In print on Phys Rev ST Accel and Beams.
- [13] B. Auchmann, R. de Maria, S. Russenschuck, and S. Kurz. 2d electromagnetic model of fast-ramping superconducting magnets. In *Proceedings of ICAP 2006, Chamonix, France, 2006*.
- [14] B. Auchmann, R. de Maria, and S. Russenschuck. Comparative study of inter-strand coupling current models for accelerator magnets. Technical Report CERN-AT-2006-11, CERN, June 2006. Presented at: European Particle Accelerator Conference EPAC'06 , Edinburgh, Scotland, UK , 26 - 30 Jun 2006.
- [15] G. Moritz, J. Kaugerts, G. J. Escallier, G. Ganetis, A. K. Jain, A. Marone, J. F. Muratore, R. Thomas, P. Wanderer, B. Auchmann, R. de Maria, S. Russenschuck, and M. Wilson. Recent test results of the fast-pulsed 4 t cos dipole gsi 001. In *Particle Accelerator Conference PAC 2005 , Knoxville, TN, USA , 16 - 20 May 2005*, page 683, May 2005.
- [16] R. de Maria. Time transient effects in superconducting magnets. Master Thesis for Università degli Studi di Roma La Sapienza, jul 2004.
- [17] P. K. Skowronski, F. Schmidt, R. de Maria, and E. Forest. New developments of mad-x using ptc. In *Proceedings of ICAP 2006*, September 2006.
- [18] R. de Maria, F. Schmidt, and P. K. Skowronski. Advances in matching with mad-x. In *Proceedings of ICAP*, September 2006.
- [19] R. de Maria, T. Kroyer, and V. Shiltsev. Field fluctuation and beam screen vibration measurements in the lhc magnets. In *Proceedings of PAC07, Albuquerque, New Mexico, USA, 2007*.